

# Improved assessment of the statistical stability of turbulent flows using extended Orr-Sommerfeld stability analysis

Vilda K. Markeviciute\* and Rich R. Kerswell†

*Department of Applied Mathematics and Theoretical Physics,  
University of Cambridge, Wilberforce Rd, Cambridge CB3 0WA, UK*

(Dated: January 6, 2022)

The concept of statistical stability is central to Malkus’s 1956 attempt to predict the mean profile in shear flow turbulence. Here we discuss how his original attempt to assess this - an Orr-Sommerfeld analysis on the mean profile - can be improved by considering a cumulant expansion of the Navier-Stokes equations. Focusing on the simplest non-trivial closure (commonly referred to as CE2) which corresponds to the quasilinearized Navier-Stokes equations, we develop an extended Orr-Sommerfeld analysis (EOS) which also incorporates information about the fluctuation field. A more practical version of this - minimally extended Orr-Sommerfeld analysis (mEOS) - is identified and tested on a number of statistically-steady and therefore statistically stable turbulent channel flows. Beyond the concept of statistical stability, this extended stability analysis should also improve the popular approach of mean-flow linear analysis in time-dependent flows by including more information about the underlying flow in its predictions.

## I. INTRODUCTION

This paper revisits the seminal work of Malkus [1] which attempted to build a theory of shear turbulence. This theory was based upon maximising the momentum transport (or equivalently dissipation rate) achieved by the flow amongst all those with a marginally-stable mean profile. Malkus clearly had a statistical form of marginal stability in mind but, to make progress, had to resort to specifying marginally with respect to the then 50-year-old Orr-Sommerfeld equation [2, 3]. So posed, his marginal stability idea was quickly repudiated [4] (and more recently [5]) although further studies showed it could be made to work if eddy rather than molecular diffusion was used [6–9]. The concept of statistical stability was, however, central to Malkus’s thinking (remaining so throughout his career [10, 11]) and is clearly different from stability as viewed within the context of the governing Navier-Stokes equations (epitomised by the celebrated Orr-Sommerfeld equation). For example, it is fairly uncontentious to assert that the turbulent attractor in, say, pressure-driven channel flow has stationary statistics (defined by averaging over one or more homogeneous directions or in an ensemble sense) and so within the partial differential equations which govern how these statistics evolve, the realised turbulence is a stable fixed point - i.e. turbulence is *statistically* stable to infinitesimal perturbations of the statistics. This is in contrast to the time-dependent turbulent attractor as viewed in the Navier-Stokes equations where adding a small disturbance may well see that disturbance grow and never decay yet the original statistics still recover (we show an example of this below). The difference, of course, is that a flow disturbance can have a component along the turbulent trajectory and hence acts as a time-shift: this part of the disturbance never decays to zero but does not affect the statistics [e.g. 12]. For his theory, Malkus wanted a statistical stability criterion based only on the lowest order statistic - the mean flow. Clearly more statistical information needs to be incorporated and it is our objective here to attempt this. At the very least, doing so should improve the now-standard approach of carrying out linear stability analysis of the mean profile of time-dependent flows in an attempt to understand observed coherent structures [e.g. 13–23].

The motivation for this work comes from two different directions. The first is the general approach of applying linear analysis around the mean profile of a time-varying, possibly turbulent flow to deduce information about the likely fluctuations seen. Initially, this took the form of linear stability analysis stimulated by Malkus’s work which tends to work well in free-shear turbulent flows like jets where inviscid (inflectional) instabilities dominate [13–15] but less well in wall-bounded situations where viscosity is important (although there can be successes [e.g. 17, 18, 22]). Driven by the fact that shear flow mean profiles tend to be linearly stable, this approach subsequently diversified into non-modal analysis [24–26] and input-output or resolvent analyses [27–35]. The resolvent approach has been particularly illuminating in showing exactly how far linear analysis can go given the mean flow profile [36]. Predictions can be made of the dominant fluctuation response at a given frequency and wavevector which typically resonates with observations at least up to amplitude and phase. In some sense this solves ‘half’ the problem of turbulence - given a mean flow, linear analysis around this can extract the dominant fluctuation structures - and refocuses attention on the ‘other’ half - predicting the mean profile. Identifying the required amplitudes and phases of the all fluctuation fields to support the observed mean profile, however, may approach the difficulty of ‘just’ solving the Navier-Stokes equations.

\* vkm28@cam.ac.uk

† r.r.kerswell@damtp.cam.ac.uk

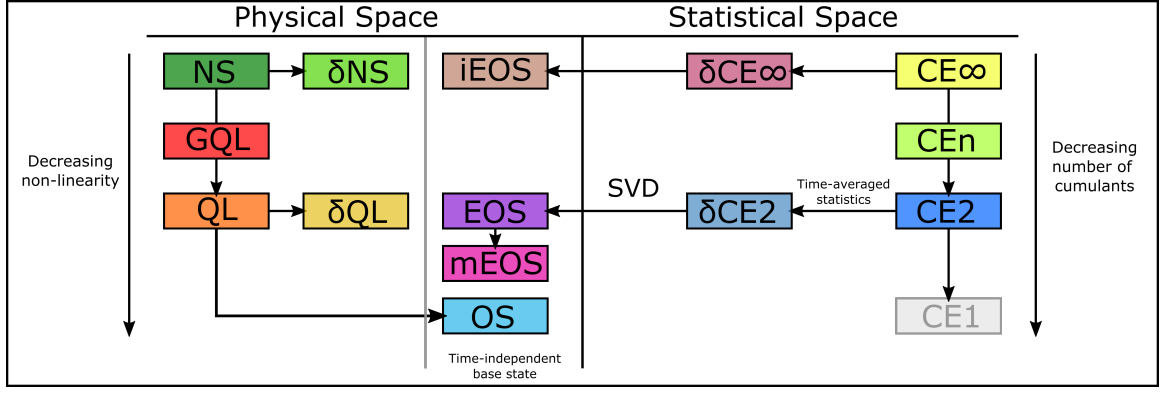


FIG. 1: Diagram of the various approaches to the stability of turbulent states showing the path to the Extended Orr-Sommerfeld analysis (EOS). Physical space (methods are ordered top to bottom by decreasing non-linearity): Full Navier-Stokes equations (NS) and their linear perturbation equations ( $\delta NS$ ), Generalised Quasi-Linear approximation (GQL), Quasi-Linear approximation (QL) and the perturbed equations ( $\delta QL$ ), Orr-Sommerfeld equation around a turbulent mean velocity profile (OS), Extended, minimal Extended and infinitely Extended Orr-Sommerfeld equations (EOS, mEOS, iEOS). Statistical space (methods are ordered top to bottom in decreasing number of statistical cumulants maintained): CEn equations which include order  $n$  statistical cumulant expansion with their perturbed equations  $\delta CEn$ . Special cases for  $n = 2$  (second order expansion) and  $n = \infty$  (infinite expansion) are emphasised.

One alternative is to appeal to some simpler ‘organising’ physical principle as epitomised in [1] and then the idea of statistical stability seems a key concept.

The second motivation is the resurgence of interest in dealing with statistical quantities directly through a cumulant expansion of time-varying flows [37–39]. Generating the evolution equations for cumulants immediately highlights the closure problem of turbulence in which the time-derivative of a  $n$ th-order cumulant requires knowledge of the  $(n+1)$ th cumulant and so forth. Present-day computational power has, however, renewed interest in the pursuit of simple cumulant-discard closures to see how well they do in modelling flows in a variety of contexts: e.g. in atmospheric dynamics [40–44]; astrophysics [45]; plasmas [46, 47] and wall-bounded shear flows [48–50]. The most popular closure ignores third and higher order cumulants - commonly referred to as CE2 - and has the nice property of being exact for a quasilinear (or historically a ‘mean field theory’) version of the Navier-Stokes equations. Significantly for our purposes here, CE2 and higher closures ( $CEn$  where  $n \geq 3$  is the highest order cumulant retained) present the most natural framework in which to extend Malkus’s idea of statistical stability. In what follows, the focus will be on using CE2 and its relationship to the quasilinear version of the Navier-Stokes equations to develop an improved version of the usual Orr-Sommerfeld analysis (or ‘OS analysis’ for short) of the mean profile: see Figure 1.

The plan of this paper is to illustrate the analysis within the context of channel flow described in section II. Throughout, the averaging procedure used will be streamwise ( $x$ ) and spanwise ( $z$ ) averaging so that the mean flow  $\mathbf{U} = U(y, t)\hat{\mathbf{x}}$  depends only on the cross-stream variable  $y$  and time. Malkus pointedly only chose a spanwise average so that his mean profile  $\mathbf{U} = U(x, y, t)\hat{\mathbf{x}}$  could depend on the cross-stream *and* streamwise variables. As a result, his Orr-Sommerfeld analysis targeted the stability of a streamwise-independent mean profile  $U(y)\hat{\mathbf{x}}$  to streamwise-dependent *mean flow* disturbances  $\delta U(y)\exp(ik(x - ct))$  rather than fluctuation fields defined as having non-vanishing spanwise dependence. Contrarily, there are growing arguments to only streamwise average to retain the spanwise structure of the mean flow, i.e.  $\mathbf{U} = U(y, z, t)\hat{\mathbf{x}}$  (e.g. see Table 1 of [51] for a sample list of relevant works). Despite this, the focus here is on the simplest mean flow definition  $\mathbf{U} = U(y, t)\hat{\mathbf{x}}$  given the central role this plays in resolvent flow analysis but, there’s no doubt, extending the mean flow definition is clearly an important direction to extend the approach discussed here. Standard Orr-Sommerfeld analysis is recalled in section II A.

Section II B then introduces the cumulant expansion approach [37–39] and the hierarchy of evolution equations for these statistical quantities. Solving these equations to (hopefully) reach a steady state is an appealingly direct way to estimate the properties of statistically steady turbulent flows since it avoids having to average across large DNS-generated datasets. Here, however, the emphasis is on the concept of stability in this statistical framework and its relationship to (dynamic) stability within the Navier-Stokes equations (see section II C) *not* on the accuracy of suitable closures of the cumulant equations in capturing the reference flow state. Our particular focus will be on the simplest non-trivial cumulant-discard scheme CE2 given the rapidly increasing dimensionality of the approach:  $CEn$  works with cumulants up to order  $n$  which, before exploiting any symmetries, is typically a  $3n-2$  rank tensor (3 spatial coordinates per field reduced by 2 averaging directions). CE2 is exact for the quasilinearized Navier-Stokes equations - or QL equations - and translating what a statistically-steady state in CE2 means for the QL equations is a crucial step discussed in §II D. An equally important discussion then follows in §II E where the subsequent stability predictions within the CE2 and QL systems are compared. Quasilinearization [52–54] has enjoyed a resurgence of interest recently [e.g. 55–57] given its accessibility, and together with its ‘generalised’ elaboration [58] in which the definition of

what constitutes a mean is extended, has the ability to focus on different parts of the nonlinearity in the Navier-Stokes equations [e.g 59].

Section III A then introduces an extended version of Orr-Sommerfeld analysis - or ‘EOS’ analysis - based on translating the statistical stability problem in CE2 back to the dynamical equations. Intriguingly, this is *not* the same as just working within the QL approximation (as §II E makes clear). Applying EOS analysis carries a substantial overhead so we consider a reduced (practical) version referred to as ‘minimally extended Orr-Sommerfeld analysis’ - or ‘mEOS’ analysis - in section III B which is almost as cheap to apply as OS analysis.

Interestingly, applying the same strategy of mapping a cumulant-based system back to the underlying dynamical equations can only go one level higher in sophistication and requires a jump directly to CE $\infty$ . This transforms EOS into the familiar linearised Navier-Stokes equations albeit based around the steady base state derived by assuming stationary 2nd rank cumulants. This ‘infinitely extended Orr-Sommerfeld’ analysis is described in §III B. Section IV then explores the performance of OS, EOS and mEOS analyses on 4 different turbulent states realised in 2D channel flow. The limitations of the analysis are discussed in §V followed by a summary and final thoughts in section §VI.

## II. FORMULATION: CHANNEL FLOW

For context in this work we consider channel flow  $\mathbf{u}^*(\mathbf{x}^*, t^*)$  of a fluid with density  $\rho^*$  and kinematic viscosity  $\nu^*$  between two parallel plates at  $y^* = \pm h^*$  across which a pressure gradient  $9\rho^* U^{*2} G(t^*)/4h^* \hat{\mathbf{x}}$  is imposed such that the bulk flow

$$U^* := \frac{1}{2h} \int_{-h}^h \mathbf{u}^* dy^* \quad (1)$$

is kept constant (unstarred/starred quantities are dimensionless/dimensional). Non-dimensionalizing the Navier-Stokes equations using  $h^*$ ,  $3U^*/2$  (so Reynolds numbers based on the bulk speed and the laminar centreline speed  $U^{*c} = 3U^*/2$  correspond [60]) and  $\rho^*$  leads to

$$\begin{aligned} \mathbf{u}_t + \mathbf{u} \cdot \nabla \mathbf{u} &= G(t) \hat{\mathbf{x}} - \nabla p + \frac{1}{Re} \nabla^2 \mathbf{u} \\ \nabla \cdot \mathbf{u} &= 0 \end{aligned} \quad (2)$$

with  $\frac{1}{2} \int_{-1}^1 u dy = 2/3$  where  $\mathbf{u} = \mathbf{u}^*/U^* = u\hat{\mathbf{x}} + v\hat{\mathbf{y}} + w\hat{\mathbf{z}}$ ,  $t = 3U^*/(2h^*)t^*$  and  $Re := 3U^*h^*/2\nu^*$ . We consider a (non-dimensionalised) flow domain  $(x, y, z) \in [-L_x, L_x] \times [-1, 1] \times [-L_z, L_z]$  with non-slip boundary conditions on the plates at  $y = \pm 1$  and periodic conditions in the streamwise  $x$  and spanwise  $z$  directions (fundamental wavenumbers are labelled  $\alpha := \pi/L_x$  and  $\beta := \pi/L_z$ ). Defining the averaging process as

$$\overline{(\cdot)} := \frac{1}{4L_x L_z} \int_{-L_x}^{L_x} \int_{-L_z}^{L_z} (\cdot) dx dz, \quad (3)$$

the flow can be decomposed into a mean  $U(y, t) \hat{\mathbf{x}} := \overline{\mathbf{u}(\mathbf{x}, t)}$  and fluctuation part  $\tilde{\mathbf{u}} := \mathbf{u} - \bar{\mathbf{u}} = \tilde{u}\hat{\mathbf{x}} + \tilde{v}\hat{\mathbf{y}} + \tilde{w}\hat{\mathbf{z}}$  (due to symmetry, a vanishing mean spanwise component is assumed so  $(\tilde{v}\tilde{w})_y = 0$ ). The Navier-Stokes equations can be similarly decomposed into a mean part,

$$U_t - \frac{1}{Re} U_{yy} = G - (\tilde{u}\tilde{v})_y \quad (4)$$

and a fluctuation part,

$$\tilde{\mathbf{u}}_t = \frac{1}{Re} \nabla^2 \tilde{\mathbf{u}} - \nabla \tilde{p} - U \tilde{\mathbf{u}}_x - \tilde{v} U_y \hat{\mathbf{x}} - (\tilde{\mathbf{u}} \cdot \nabla \tilde{\mathbf{u}} - \overline{\tilde{\mathbf{u}} \cdot \nabla \tilde{\mathbf{u}}}), \quad (5)$$

which is incompressible

$$\nabla \cdot \tilde{\mathbf{u}} = 0 \quad (6)$$

where subscripts denote derivatives (e.g.  $U_y = dU/dy$ ).

### A. Orr-Sommerfeld stability analysis

Given a possibly turbulent flow  $(U, \tilde{\mathbf{u}})$ , the ‘standard’ Orr-Sommerfeld analysis - ‘OS analysis’ for short - is to consider small (a.k.a. infinitesimal) perturbations  $(0, \delta\tilde{\mathbf{u}})$  to a base state  $(U, \mathbf{0})$  where the fluctuation field is ignored and the mean flow  $U$  is assumed steady or further time-averaged to make it so. As a result only the equations (5) and (6) need be perturbed (and hence linearised) and since  $U = U(y)$ , the ensuing eigenvalue calculation is parametrised by a streamwise and spanwise wavenumber. Squires theorem [61] is usually invoked to focus the search for instability to spanwise-independent perturbations and leads to the celebrated Orr-Sommerfeld equation [2, 3]. In primitive variables,  $\tilde{w}$  then decouples from  $\tilde{u}$  and  $\tilde{v}$  and can be ignored, leaving the reduced eigenproblem

$$-im\alpha c \tilde{u} = \frac{1}{Re}(\tilde{u}_{yy} - m^2 \alpha^2 \tilde{u}) - im\alpha \tilde{p} - im\alpha U \tilde{u} - U_y \tilde{v}, \quad (7)$$

$$-im\alpha c \tilde{v} = \frac{1}{Re}(\tilde{v}_{yy} - m^2 \alpha^2 \tilde{v}) - \tilde{p}_y - im\alpha U \tilde{v}, \quad (8)$$

$$0 = im\alpha \tilde{u} + \tilde{v}_y \quad (9)$$

where  $(\tilde{u}, \tilde{v}, \tilde{p}) \propto e^{im\alpha(x-ct)}$  and  $c := c_r + ic_i$  is the (complex) eigenvalue. The (matrix) size of the eigenproblem is only  $3N_y \times 3N_y$  for each streamwise wavenumber  $m$  and so needs to be repeated  $N_x$  times ( $N_x, N_y$  represent the streamwise and wall-normal truncations). When the mean profile is known from simulations or experiments, for typical resolutions, this is an easily accessible procedure which through the structure of the most unstable eigenvectors can shed some light on the dominant structures of the turbulent flow.

### B. Statistics: cumulants

In this section we consider a statistical framework for the flow by working with the equal-time cumulants of the flow [37–39]. Even within this framework, we specialise further to exclusively consider equal  $x$  &  $z$  cumulants which are the subset of cumulants which influence the mean flow. The first cumulant is the mean  $U(y, t)$ . The second cumulant is the symmetric matrix

$$\mathbf{C}(y_1, y_2, t) := \overline{\tilde{\mathbf{u}}(x, y_1, z, t) \otimes \tilde{\mathbf{u}}(x, y_2, z, t)} = \begin{pmatrix} C_{11} & C_{12} & C_{13} \\ C_{21} & C_{22} & C_{23} \\ C_{31} & C_{32} & C_{33} \end{pmatrix}, \quad (10)$$

where we introduce the notation  $C_{ij}(1, 2) := \overline{[\tilde{\mathbf{u}}(x, y_1, z, t)]_i [\tilde{\mathbf{u}}(x, y_2, z, t)]_j}$  (here  $[\tilde{\mathbf{u}}]_1 = \tilde{u}$ ,  $[\tilde{\mathbf{u}}]_2 = \tilde{v}$  and  $[\tilde{\mathbf{u}}]_3 = \tilde{w}$ ) to emphasize the  $y$  arguments and de-emphasize the implicit time dependence, and the third cumulant is the third order tensor

$$C_{ijk}^{(3)}(1, 2, 3) := \overline{[\tilde{\mathbf{u}}(x, y_1, z, t)]_i [\tilde{\mathbf{u}}(x, y_2, z, t)]_j [\tilde{\mathbf{u}}(x, y_3, z, t)]_k}. \quad (11)$$

These correspond to the second and third central moments of the flow respectively. Cumulants and central moments, however, diverge at fourth order and beyond, e.g.

$$C_{ijkl}^{(4)}(1, 2, 3, 4) := \overline{[\tilde{\mathbf{u}}(x, y_1, z, t)]_i [\tilde{\mathbf{u}}(x, y_2, z, t)]_j [\tilde{\mathbf{u}}(x, y_3, z, t)]_k [\tilde{\mathbf{u}}(x, y_4, z, t)]_l} \quad (12)$$

$$- C_{ij}(1, 2)C_{kl}(3, 4) - C_{ik}(1, 3)C_{jl}(2, 4) - C_{il}(1, 4)C_{jk}(2, 3). \quad (13)$$

We will not go this high in the cumulant expansion used here but just note that the  $n^{\text{th}}$  order cumulant is  $n$ -dimensional in space so that storage when doing computations becomes prohibitive very quickly. Hence the onus is on applying some sort of closure as soon as possible.

To derive evolution equations for the cumulants, we introduce a double Fourier series representation of the flow

$$\tilde{\mathbf{u}}(x, y, z, t) := \sum_m \sum_n \tilde{\mathbf{u}}^{mn}(y, t) e^{im\alpha x + in\beta z} \quad (14)$$

where  $m, n \in \mathbb{Z}$ . Clearly  $\tilde{\mathbf{u}}^{-m-n} = \tilde{\mathbf{u}}^{*mn}$  (the complex conjugate of  $\tilde{\mathbf{u}}^{mn}$ ) for a real flow but it will be clearer not to build this into the notation in anticipation of deriving perturbation equations later. Hence, we write

$$C_{ij}(1, 2) = \sum_m \sum_n \left\{ C_{ij}^{mn}(1, 2) := [\tilde{\mathbf{u}}^{mn}(y_1, t)]_i [\tilde{\mathbf{u}}^{-m-n}(y_2, t)]_j \right\} \quad (15)$$

$$C_{ijk}^{(3)}(1, 2, 3) = \sum_m \sum_n \left\{ C_{ijk}^{(3)mn}(1, 2, 3) := \sum_p \sum_q [\tilde{\mathbf{u}}^{mn}(y_1, t)]_i [\tilde{\mathbf{u}}^{pq}(y_2, t)]_j [\tilde{\mathbf{u}}^{-(m+p)-(n+q)}(y_3, t)]_k \right\} \quad (16)$$



(note e.g.  $C_{ij}^{mn}(1,2) = C_{ji}^{-m-n}(2,1)$ ). Equations to evolve the cumulants are obtained by temporally differentiating their definitions in (15) and (16) and using (5). For example, for the second order cumulant,

$$\begin{aligned} \partial_t C_{ij}^{mn}(1,2) &= [\tilde{\mathbf{u}}^{mn}(y_1,t)]_i \partial_t [\tilde{\mathbf{u}}^{-m-n}(y_2,t)]_j + \partial_t [\tilde{\mathbf{u}}^{mn}(y_1,t)]_i [\tilde{\mathbf{u}}^{-m-n}(y_2,t)]_j, \\ &= \frac{1}{Re} (\partial_1^2 + \partial_2^2 - 2m^2\alpha^2 - 2n^2\beta^2) C_{ij}^{mn}(1,2) - \begin{bmatrix} -im\alpha \\ \partial_2 \\ -in\beta \end{bmatrix}_j C_{i4}^{mn}(1,2) - \begin{bmatrix} im\alpha \\ \partial_1 \\ in\beta \end{bmatrix}_i C_{4j}^{mn}(1,2) \\ &\quad + im\alpha [U(2) - U(1)] C_{ij}^{mn}(1,2) - U_y(2) C_{i2}^{mn}(1,2) \delta_{1j} - U_y(1) C_{2j}^{mn}(1,2) \delta_{i1} \\ &\quad - \begin{bmatrix} -im\alpha \\ \partial_2 \\ -in\beta \end{bmatrix}_k C_{ijk}^{(3)mn}(1,2,2) - \begin{bmatrix} im\alpha \\ \partial_1 \\ in\beta \end{bmatrix}_k C_{ikj}^{(3)-m-n}(2,1,1) \end{aligned} \quad (17)$$

where  $\partial_i := \partial_{y_i}$  and  $C_{i4}^{mn}(1,2) := [\tilde{\mathbf{u}}^{mn}(y_1,t)]_i \tilde{p}^{-m-n}(y_2,t) =: C_{4i}^{-m-n}(2,1)$  are 3 extra ‘velocity-pressure’ cumulants that get generated. Incompressibility conditions give the required 3 extra matrix constraints

$$\begin{bmatrix} im \\ \partial_1 \\ in \end{bmatrix}_i C_{ij}^{mn}(1,2) = 0 \quad j \in \{1,2,3\} \quad (18)$$

along with the equation for the mean equation (4)

$$U_t - \frac{1}{Re} U_{yy} = G - \sum_m \sum_n \partial_y C_{12}^{mn}(y,y,t) \quad (19)$$

to close the system. The infamous closure problem of the Navier-Stokes equation is immediately evident here in that the evolution equation for the 2nd order cumulant depends on the 3rd order cumulant, a pattern which continues for higher order cumulants so the system never closes. A popular (lowest) closure - commonly called CE2 - is to simply ignore the 3rd order cumulant which is equivalent to ignoring the fluctuation-fluctuation term (last bracketed term on the rhs of (5)). This is the quasilinear approximation or sometimes referred to as mean field theory [e.g. 52–54].

$$U_t = \frac{1}{Re} U_{yy} + G - (\tilde{u}\tilde{v})_y \quad (20)$$

$$\tilde{\mathbf{u}}_t = \frac{1}{Re} \nabla^2 \tilde{\mathbf{u}} - \nabla \tilde{p} - U \tilde{\mathbf{u}}_x - \tilde{v} U_y \hat{\mathbf{x}}, \quad (21)$$

$$0 = \nabla \cdot \tilde{\mathbf{u}} \quad (22)$$

The defining feature of this approximation is that (21) is linear in  $\tilde{\mathbf{u}}$  so that fluctuations with different wavenumbers are only coupled in the mean flow equation (20). This linearity also means that any fluctuation field (parametrised by streamwise and spanwise wavenumber) can not be consistently in the stable manifold of  $U$  as it varies with time. In particular, if  $U$  is steady, only marginally-stable fluctuation fields can exist. Malkus argued for this model (and its marginal stability implications) on the basis that the fluctuation-fluctuation nonlinear term was only stabilising. This would be reasonable if bifurcations from unidirectional shear flows were always supercritical but, some decades later, subcriticality has been realised the more generic situation [62–65].

Applying a closure at next order so  $C^{(4)}$  is some assumed function of the lower cumulants or simply ignored (termed CE3) is less straightforward as the ensuing positive definiteness of the second cumulant is not automatic [66]. This difficulty explains the popularity of the lower-order CE2 approximation.

### C. Approximations to Statistical Stability

The approach here is to consider the stability within the cumulant framework as this presents a natural way to assess stability of the flow statistics. Ideally, this should be attempted for a cumulant expansion which is high enough order to show a robustness against including even higher order cumulants. However, the rate at which the dimensionality of this procedure explodes means that only second and perhaps third order closures are currently practical. As a result, we focus on CE2 here and identify a clear way to progress to higher order (see §III B)

CE2 is the statistical equations (17)–(19) with the third order cumulants in (17) set to zero. The corresponding equations for

perturbations  $(\delta U, \delta C_{ij}^{mn})$  upon a base statistical state  $(U, C_{ij}^{mn})$  - called the  $\delta$ CE2 problem - are

$$\begin{aligned} \partial_t \delta C_{ij}^{mn}(1,2) = & \frac{1}{Re} (\partial_1^2 + \partial_2^2 - 2m^2\alpha^2 - 2n^2\beta^2) \delta C_{ij}^{mn}(1,2) - \begin{bmatrix} -im\alpha \\ \partial_2 \\ -in\beta \end{bmatrix}_j \delta C_{i4}^{mn}(1,2) - \begin{bmatrix} im\alpha \\ \partial_1 \\ in\beta \end{bmatrix}_i \delta C_{4j}^{mn}(1,2) \\ & + im\alpha [U(2) - U(1)] \delta C_{ij}^{mn}(1,2) - U_y(2) \delta C_{i2}^{mn}(1,2) \delta_{1j} - U_y(1) \delta C_{2j}^{mn}(1,2) \delta_{i1} \\ & + im\alpha [\delta U(2) - \delta U(1)] C_{ij}^{mn}(1,2) - \delta U_y(2) C_{i2}^{mn}(1,2) \delta_{1j} - \delta U_y(1) C_{2j}^{mn}(1,2) \delta_{i1} \end{aligned} \quad (23)$$

$$0 = \begin{bmatrix} im\alpha \\ \partial_1 \\ in\beta \end{bmatrix}_i \delta C_{ij}^{mn}(1,2), \quad (24)$$

$$\partial_t \delta U = \frac{1}{Re} \delta U_{yy} + \delta G - \sum_m \sum_n \partial_y \delta C_{12}^{mn}(y, y, t). \quad (25)$$

If the pressure gradient is kept fixed  $\delta G = 0$ , otherwise the constant volume flux condition  $\int_{-1}^1 \delta U dy = 0$  is the extra constraint required. Crucially the ansatz  $(\delta U, \delta C_{ij}^{mn}) \propto e^{it}$  is possible if the base state is taken to be independent of time - in other words the base flow is *statistically steady*.

Even in the cheapest 2D situation, the CE2 stability problem requires handling  $5N_x$  correlation matrices of size  $N_y^2$  all linked through the mean equation. This leads to a matrix of size  $(N_y + 5N_x N_y^2)^2$  or  $\approx 25N_x^2 N_y^4$  elements which is out of reach even for modest resolutions. Given this, we explore a route to potentially still capture the essence of the CE2 statistical stability approximation without the considerable cost. To do this, we discuss a connection back to the equations of motion which plausibly retains the steadiness of the stability problem.

#### D. Steady Statistics and Simplifications

The assumption of steady statistics of the base flow is a strong one, not only implying steadiness of  $C_{ij}$  overall but also individually of  $C^{mn}(1,2) := \tilde{\mathbf{u}}^{mn}(y_1, t) \otimes \tilde{\mathbf{u}}^{-m-n}(y_2, t)$  (recall its definition in (15)) to make the component equation (23) steady over all  $(m, n)$  wavenumber pairings. Given the independence of the coordinates  $y_1$  and  $y_2$ , this suggests the most general time-dependence of the underlying velocity field is  $\tilde{\mathbf{u}}^{mn}(y, t) = \tilde{\mathbf{u}}_0^{mn}(y) e^{i\Omega_{mn}(t)}$  where  $\Omega_{mn}(t)$  is some (real) phase function and then

$$C^{mn}(1,2) = \tilde{\mathbf{u}}_0^{mn}(y_1) \otimes \tilde{\mathbf{u}}_0^{-m-n}(y_2). \quad (26)$$

This is a crucial simplification in CE2 because then the associated stability problem (23)-(25) has temporally-constant coefficients and becomes a (conceptually at least) simple eigenvalue problem. In what follows below, we will not attempt to solve this directly as it is too unwieldy. Instead, a smaller, more practical QL stability problem is sought as a good proxy for it.

The key is identifying a suitable base velocity field around which to develop a QL-type stability problem. Allowing arbitrary phases  $\Omega_{mn}$  will not lead to an eigenvalue problem but retaining a constant representative frequency  $\omega_{mn} := d\Omega_{mn}/dt$  for each base wavenumber present can do (note  $\omega_{mn} = -\omega_{-m-n}$ ,  $\tilde{\mathbf{u}}_0^{mn*} = \tilde{\mathbf{u}}_0^{-m-n}$  for the base flow to be real and  $U(y) = \tilde{\mathbf{u}}_0^{00}(y)$ ). To illustrate this, we discuss the generic situation where the allowed perturbation wavenumber pairings are a subset of those present in the base flow i.e.  $\delta \tilde{\mathbf{u}}^{mn}$  is only non-zero if  $\tilde{\mathbf{u}}_0^{mn}$  is (these are Type B perturbations in the nomenclature of §II E where the general situation is discussed). In this case, the QL-type problem

$$\partial_t \delta \tilde{\mathbf{u}}^{mn} = i\omega_{mn} \delta \tilde{\mathbf{u}}^{mn} + \mathbb{L}^{mn}(U) \delta \tilde{\mathbf{u}}^{mn} + \mathbb{J}^{mn}(\delta U) \tilde{\mathbf{u}}_0^{mn} \quad \forall (m, n) \neq (0, 0) \quad (27)$$

$$\partial_t \delta U = \frac{1}{Re} \delta U_{yy} + \delta G - \sum_m \sum_n \partial_y \left\{ \tilde{u}_0^{mn} \delta \tilde{v}^{-m-n} + \delta \tilde{u}^{mn} \tilde{v}_0^{-m-n} \right\} \quad (28)$$

where

$$\mathbb{L}^{mn}(U) \tilde{\mathbf{u}}^{mn} := \frac{1}{Re} [\partial_y^2 - m^2\alpha^2 - n^2\beta^2] \tilde{\mathbf{u}}^{mn} - \begin{bmatrix} im\alpha \\ \partial_y \\ in\beta \end{bmatrix} \tilde{\mathbf{p}}^{mn} - im\alpha U \tilde{\mathbf{u}}^{mn} - \tilde{v}^{mn} U_y \hat{\mathbf{x}}, \quad (29)$$

$$\mathbb{J}^{mn}(\delta U) := \lim_{\epsilon \rightarrow 0} \frac{1}{\epsilon} [\mathbb{L}^{mn}(U + \epsilon \delta U) - \mathbb{L}^{mn}(U)] = \mathbb{L}^{mn}(U + \delta U) - \mathbb{L}^{mn}(U) \quad (30)$$

(as  $\mathbb{L}^{mn}$  is affine in  $U$ ) reproduces eigenvalues from the CE2 problem (23)-(25) provided the perturbation takes the form

$$\delta \tilde{\mathbf{u}}(x, y, z, t) = \sum_m \sum_n \left[ \delta \tilde{\mathbf{u}}^{mn}(y, t) := \delta \mathbf{v}^{mn}(y) e^{(\lambda + i\omega_{mn})t} \right] e^{i(m\alpha x + n\beta z)} \quad (31)$$

so that  $\mathbf{C}^{mn} := \tilde{\mathbf{u}}_0^{mn}(y_1, t) \otimes \delta \tilde{\mathbf{u}}^{-m-n}(y_2, t) + \delta \tilde{\mathbf{u}}^{mn}(y_1, t) \otimes \tilde{\mathbf{u}}_0^{-m-n}(y_2, t) \propto e^{\lambda t}$ . This, however, simply reduces down to the QL eigenvalue problem - or  $\delta$ QL problem

$$\lambda \delta \tilde{\mathbf{u}}^{mn} = \mathbb{L}^{mn}(U) \delta \tilde{\mathbf{u}}^{mn} + \mathbb{J}^{mn}(\delta U) \tilde{\mathbf{u}}_0^{mn} \quad \forall (m, n) \neq (0, 0) \quad (32)$$

$$\lambda \delta U = \frac{1}{Re} \delta U_{yy} + \delta G - \sum_m \sum_n \partial_y \left\{ \tilde{u}_0^{mn} \delta \tilde{v}^{-m-n} + \delta \tilde{u}^{mn} \tilde{v}_0^{-m-n} \right\} \quad (33)$$

where all the  $\omega_{mn}$  disappear although they remain in the definition of the perturbation. Hence the eigenvalues of this  $\delta$ QL problem are insensitive to the  $\omega_{mn}$  as they should be since the  $\delta$ CE2 problem (23)-(25) is ignorant of them.

Moving forward, it is therefore sufficient to set all the  $\omega_{mn} = 0$  - so the base flow  $\tilde{\mathbf{u}}_0^{mn}$  is steady and consider the  $\delta$ QL problem (32)-(33). The eigenvalues which emerge from this  $\delta$ QL problem are reproduced in the  $\delta$ CE2 problem with equivalent eigenfunctions. The implication is then that the much more tractable  $\delta$ QL problem reveals important information about the  $\delta$ CE2 problem. This realisation forms the basis for an extended version of Orr-Sommerfeld analysis. Before pursuing this, we make a remark and an observation.

The remark is that certain notational liberties have been taken here to keep the discussion as clear as possible. For example, the operator  $\mathbb{L}^{mn}$  strictly maps an incompressible flow field to another which involves a supplementary scalar field (the pressure) entering into the definition. As is well known, this is determined by imposing incompressibility. An implicitly-incompressible representation for the velocity field could be used (e.g. reducing the problem down to just using wall-normal velocity and vorticity) to avoid this wrinkle but staying with primitive variables makes the various manipulations as clear as possible.

The observation is that the special form of the nonlinearity in the QL and CE2 formulations means that different wavenumber pairings only interact through the mean flow equation. As a result eigenvalues can be sought within any subset of the wavenumbers possible and these are still valid within the full system of wavenumbers i.e. this is not a truncation merely a subclass of disturbances. In particular, for CE2 the simplest perturbation of the base state  $(U, \mathbf{C})$  just consists of perturbations in one wavenumber pairing and the mean flow,

$$(\delta U, \delta \mathbf{C}^{mn}) e^{\lambda t}. \quad (34)$$

Even this leads to an eigenvalue matrix calculation of size  $(N_y + 9N_y^2) \times (N_y + 9N_y^2)$  in 3D. The equivalent QL perturbation has to consider

$$(\delta U, \delta \tilde{\mathbf{u}}^{mn}, \delta \tilde{\mathbf{u}}^{-m-n}) e^{\lambda t} \quad (35)$$

and requires an eigenvalue matrix calculation of size  $(N_y + 8N_y) \times (N_y + 8N_y)$  which is *much* smaller (or  $(N_y + 6N_y) \times (N_y + 6N_y)$  in 2D - see Appendix A).

### E. Relationship between dynamic stability in QL and statistical stability in CE2

We now discuss more generally how the dynamic stability predictions of QL based on  $\tilde{\mathbf{u}}_0^{mn}(y)$  should be a good proxy for the statistical predictions of CE2 based upon  $\mathbf{C}^{mn}(1, 2) = \tilde{\mathbf{u}}_0^{mn}(y_1) \otimes \tilde{\mathbf{u}}_0^{-m-n}(y_2)$ . The basis for this statement is the fact to be shown below that any instability present in QL has an equivalent in CE2. The reverse statement is not necessarily true but this is a stronger statement than needed. For our purposes, we need to argue that CE2 only predicts instability if QL does. That is, CE2 can have additional modes of instability but these are only present if QL has at least one mode of instability so the predictions of the two systems are equivalent.

We define two sets which contain all the wavenumber pairings that contain energy in the base state  $\tilde{\mathbf{u}}_0$  and the perturbation field  $\delta \tilde{\mathbf{u}}$  respectively,

$$\Lambda := \left\{ (m, n) \left| \int_{-1}^1 |\tilde{\mathbf{u}}_0^{mn}|^2 dy > 0 \right. \right\} \quad \& \quad \delta \Lambda := \left\{ (m, n) \left| \int_{-1}^1 |\delta \tilde{\mathbf{u}}^{mn}|^2 dy > 0 \right. \right\}. \quad (36)$$

There are two possibilities for an eigenfunction for the linear stability problem in QL (the  $\delta$ QL problem):

- Type A:  $\delta \Lambda \subseteq \Lambda'$ , the complement of  $\Lambda$  (all possible unexcited wavenumber pairings in the base solution  $\tilde{\mathbf{u}}_0$ ).
- Type B:  $\delta \Lambda \subseteq \Lambda$  when there is an exact equivalent eigenfunction for  $\delta$ CE2 (the statistical stability problem in CE2).

Type A is the most straightforward to understand as there is no feedback of the fluctuation field onto the mean in  $\delta$ QL (the feedback is quadratic in the fluctuation disturbance). In this case, the stability problem simplifies to an Orr-Sommerfeld-type problem on the base mean profile. As a result, a Type A eigenfunction  $\delta \tilde{\mathbf{u}}_A$  in  $\delta$ QL consists of just one wavenumber pair  $(\hat{m}, \hat{n})$ . The situation is similar in CE2 with the corresponding eigenmatrix  $\delta \mathbf{C}_A = |\delta \tilde{\mathbf{u}}_A|^2$  but with two notable differences. The first is the

corresponding eigenvalue in CE2 is  $2\Re(\lambda_A)$  where  $\lambda_A$  is the QL-eigenvalue ( $\partial_t|\delta\tilde{\mathbf{u}}_A|^2 = (\lambda_A\tilde{\mathbf{u}}_A)\tilde{\mathbf{u}}_A^* + \tilde{\mathbf{u}}_A(\lambda_A^*\tilde{\mathbf{u}}_A^*) = (\lambda_A + \lambda_A^*)|\delta\tilde{\mathbf{u}}_A|^2$ ). The second is that a mean flow perturbation is forced,

$$\delta U_A = \left[ 2\Re(\lambda_A) - \frac{1}{Re} \partial_y^2 \right]^{-1} \partial_y \delta C_{A12}^{\hat{m}\hat{n}}(y, y) \quad (37)$$

(in the simpler constant-pressure gradient situation), which in turn forces perturbation components across *all* wavenumber pairings in  $\Lambda$  since

$$\delta C_{Aij}^{mn}(1, 2) = \mathcal{L}(\lambda_A)^{-1} \left[ im[\delta U_A(2) - \delta U_A(1)] C_{ij}^{mn}(1, 2) - \partial_y \delta U_A(2) C_{i2}^{mn}(1, 2) \delta_{1j} - \partial_y \delta U_A(1) C_{2j}^{mn}(1, 2) \delta_{i1} \right] \quad (38)$$

where  $\mathcal{L}(\lambda_A)$  is the spatial operator defined by the system (23) and (24) with  $\partial_t$  replaced by  $\lambda_A$ . Importantly if a Type A QL eigenvalue is unstable - i.e.  $\Re(\lambda_A) > 0$  then so is the corresponding CE2 eigenfunction.

The eigenvalue problem for Type B is more complicated since it involves multiple wavenumber pairs coupled to a mean field perturbation. However, it is straightforward to see that a Type B eigenfunction in  $\delta\mathbf{QL}$ ,

$$\left[ \delta U_B(y, t), \delta \tilde{\mathbf{u}}_B(x, y, z, t) \right] = \left[ \delta U_B(y), \sum_{(m,n) \in \delta\Lambda \subseteq \Lambda} \delta \mathbf{v}_B^{mn}(y) e^{i(m\alpha x + n\beta z)} \right] e^{\lambda_B t} \quad (39)$$

with eigenvalue  $\lambda_B$  corresponds to the eigenfunction

$$\left[ \delta U_B, \delta \mathbf{C}_B(y_1, y_2) \right] = \sum_{(m,n) \in \delta\Lambda \subseteq \Lambda} \delta \mathbf{C}_B^{mn}(y_1, y_2) := \tilde{\mathbf{u}}_0^{mn}(y_1) \otimes \delta \tilde{\mathbf{u}}_B^{-m-n}(y_2) + \delta \tilde{\mathbf{u}}_B^{mn}(y_1) \otimes \tilde{\mathbf{u}}_0^{-m-n}(y_2) \Big] e^{\lambda_B t} \quad (40)$$

with same eigenvalue in the CE2 system. There are no hybrid eigenfunctions in  $\delta\mathbf{QL}$  with  $\delta\Lambda \not\subseteq \Lambda$  as those wavenumber pairs not in  $\Lambda$  simply decouple even if they have the same eigenvalue (which is then degenerate).

It is worth briefly illustrating this partitioning into Type A and Type B perturbations in a simple example. Let  $q(x, t) := \bar{q}(t) + q'(x, t)$  over the periodic domain  $x \in [-\pi, \pi]$  where  $\overline{(\cdot)} = \frac{1}{2\pi} \int_{-\pi}^{\pi} (\cdot) dx$  so  $\overline{q'} = 0$  (and we assume  $q'(-x) = q'(x)$  for simplicity) then consider the QL-like system

$$\dot{\bar{q}} + \frac{1}{Re} \bar{q} - \frac{3}{Re^2} = -2\overline{q'^2} = -\sum_{n=1}^{\infty} q_n'^2 \quad \text{where} \quad q' := \sum_{n=1}^{\infty} q_n'(t) \cos nx \quad (41)$$

$$\dot{q}_n' = \left[ \bar{q} - \frac{n^2}{2Re} \right] q_n' \quad n = 1, 2, \dots \quad (42)$$

where the mean flow is forced by an ‘imposed pressure gradient’  $3/Re^2$ , there are the usual dissipation terms and quadratic feedback of the fluctuations onto the mean. There are multiple steady states: we choose to linearise around

$$\bar{q} = \frac{2}{Re}, \quad q_2' = \frac{1}{Re}, \quad q_n' = 0 \quad n \neq 2. \quad (43)$$

which leads to the linear perturbation equations

$$\dot{\delta \bar{q}} = -\frac{1}{Re} \delta \bar{q} - 2q_2' \delta q_2', \quad (44)$$

$$\delta \dot{q}_2' = q_2' \delta \bar{q}, \quad (45)$$

$$\delta \dot{q}_n' = \left[ \bar{q} - \frac{n^2}{2Re} \right] \delta q_n' \quad n \neq 2. \quad (46)$$

These highlight the difference between ‘new’ wavenumbers ( $n \neq 2$ ) and ‘already-present’ wavenumbers ( $n = 2$ ). Using the base flow and restricting to the perturbation to just  $n \in \{1, 2\}$ , then

$$\frac{d}{dt} \begin{bmatrix} \delta \bar{q} \\ \delta q_1' \\ \delta q_2' \end{bmatrix} = \begin{bmatrix} -\frac{1}{Re} & 0 & -2q_2' \\ 0 & \bar{q} - \frac{1}{2Re} & 0 \\ q_2' & 0 & 0 \end{bmatrix} \begin{bmatrix} \delta \bar{q} \\ \delta q_1' \\ \delta q_2' \end{bmatrix} = \frac{1}{Re} \begin{bmatrix} -1 & 0 & -2 \\ 0 & \frac{3}{2} & 0 \\ 1 & 0 & 0 \end{bmatrix} \begin{bmatrix} \delta \bar{q} \\ \delta q_1' \\ \delta q_2' \end{bmatrix} \quad (47)$$

The associated *statistical equations* for  $\bar{q}$  and  $C := \overline{q'^2}$  are

$$\dot{\bar{q}} + \frac{1}{Re} \bar{q} = \frac{3}{Re^2} - 2C = \frac{3}{Re^2} - \sum_{n=1}^{\infty} C_n \quad \text{where} \quad C_n := q_n'^2 \quad (48)$$

$$\dot{C}_n = 2 \left[ \bar{q} - \frac{n^2}{2Re} \right] C_n \quad n = 1, 2, \dots \quad (49)$$

The basic state in this formulation is  $\bar{q} = 2/Re$  and  $C_2 = 1/Re^2$  (all other  $C_n = 0$ ) and the linear ‘statistical’ stability equations (again just for  $n \in \{1, 2\}$ ) are

$$\delta \dot{\bar{q}} = -\frac{1}{Re} \delta \bar{q} - \delta C_1 - \delta C_2, \quad (50)$$

$$\delta \dot{C}_2 = 2C_2 \delta \bar{q}, \quad (51)$$

$$\delta \dot{C}_1 = 2\left[\bar{q} - \frac{1}{2Re}\right] \delta C_1. \quad (52)$$

This leads to the problem

$$\frac{d}{dt} \begin{bmatrix} \delta \bar{q} \\ Re \delta C_1 \\ Re \delta C_2 \end{bmatrix} = \frac{1}{Re} \begin{bmatrix} -1 & -1 & -1 \\ 0 & 3 & 0 \\ 2 & 0 & 0 \end{bmatrix} \begin{bmatrix} \delta \bar{q} \\ Re \delta C_1 \\ Re \delta C_2 \end{bmatrix} \quad (53)$$

which is similar but different to that in (47). Ignoring the factor of  $1/Re$ , the ‘QL’ eigenvalues are  $\lambda_A = 3/2$  (Type A),  $\lambda_B = \frac{1}{2}(-1 + i\sqrt{7})$  and  $\lambda_B^*$  (Type B) with corresponding eigenvectors (respectively)

$$\begin{bmatrix} 0 \\ 1 \\ 0 \end{bmatrix}, \quad \begin{bmatrix} \lambda_B \\ 0 \\ 1 \end{bmatrix} \quad \& \quad \begin{bmatrix} \lambda_B^* \\ 0 \\ 1 \end{bmatrix} \quad (54)$$

whereas the ‘CE2’ eigenvalues are  $2\Re(\lambda_A) = 3$  (Type A),  $\lambda_B$  and  $\lambda_B^*$  (Type B) with eigenvectors (respectively)

$$\frac{1}{\lambda_A^2 + \lambda_A + 2} \begin{bmatrix} -2 \\ \lambda_A^2 + \lambda_A + 2 \\ -\lambda_A \end{bmatrix}, \quad \begin{bmatrix} \frac{1}{2}\lambda_B \\ 0 \\ 1 \end{bmatrix} \quad \& \quad \begin{bmatrix} \frac{1}{2}\lambda_B^* \\ 0 \\ 1 \end{bmatrix} \quad (55)$$

This example shows: a) the partitioning of the perturbations into Type A and Type B, and that b) CE2 has double the corresponding Type A QL eigenvalue (as it is real) and the corresponding CE2 eigenfunction contains other forced components beyond the new wavenumber  $n = 1$ . However, these extra components, which get excited in QL at (next) quadratic order, are passive and don’t affect the eigenvalue.

Now we discuss how the  $\delta$ QL problem is a strict subset of the  $\delta$ CE2 problem. Things are clearest for the  $\delta$ CE2 Type A case where the eigenvalue problem is solely determined by the statistical stability equation for the 2nd rank cumulant,

$$\partial_t \delta C_{ij}^{mn}(1, 2) = [\tilde{\mathbf{u}}^{mn}(y_1, t)]_i \left[ \mathbb{L}_2^{mn}(U) \delta \tilde{\mathbf{u}}^{-m-n}(y_2, t) \right]_j + \left[ \mathbb{L}_1^{mn}(U) \delta \tilde{\mathbf{u}}^{mn}(y_1, t) \right]_i [\tilde{\mathbf{u}}^{-m-n}(y_2, t)]_j \quad (56)$$

$$0 = \begin{bmatrix} im \\ \partial_1 \\ in \end{bmatrix}_i \delta C_{ij}^{mn}(1, 2) \quad (57)$$

Now if  $\mathbf{e}^{(p)}$  is the  $p^{th}$  eigenfunction to the Orr-Sommerfeld problem with corresponding eigenvalue  $\lambda_p$ , it is straightforward to see that  $C_{ij}(1, 2) = \mathbf{e}_i^{(p)}(1) \mathbf{e}_j^{*(p)}(2)$  is a eigenfunction of (56)-(57) with the corresponding eigenvalue  $\lambda_p + \lambda_p^* = 2\Re(\lambda_p)$  as already mentioned (just above (37)). Less clear but still true is the fact that  $C_{ij}(1, 2) = \mathbf{e}_i^{(p)}(1) \mathbf{e}_j^{*(q)}(2)$  is also an eigenfunction with eigenvalue  $\lambda_p + \lambda_q^*$  which has no counterpart in the Orr-Sommerfeld problem as it does not correspond to one physical flow field (note it has also forced components via equations (37) and (38)). This has the consequence that CE2 has at least the number of unstable directions as the OS problem and probably more since an unstable eigenvalue linearly combined with a weakly stable eigenvalue could produce a new unstable direction. That is, if the OS problem is unstable so is CE2 and vice versa. A simple example makes this clear: consider the QL (fluctuation) system  $\dot{x} = 2x$  and  $\dot{y} = -y$  which has 1 stable and 1 unstable direction. The equivalent CE2 system where  $C_{xx} := x^2$ ;  $C_{xy} = C_{yx} := xy$  and  $C_{yy} := y^2$  (and the symmetry  $C_{xy} = C_{yx}$  built in)

$$\partial_t \begin{bmatrix} C_{xx} \\ C_{xy} \\ C_{yy} \end{bmatrix} = \begin{bmatrix} 4 & 0 & 0 \\ 0 & 1 & 0 \\ 0 & 0 & -2 \end{bmatrix} \begin{bmatrix} C_{xx} \\ C_{xy} \\ C_{yy} \end{bmatrix} \quad (58)$$

has 2 unstable and one stable. The point is in CE2, it is possible to have a perturbation of form  $[0 \ 1 \ 0]^T$  in the extra unstable direction but this perturbation has no equivalent in the OS problem as it is inconsistent with any one choice of  $x$  and  $y$ . This feature holds for any Type A perturbation in CE2 as long as the corresponding velocity is a vector i.e. there is non-trivial structure in the cross-stream direction (this was absent by design in the previous example (41)-(42)). This is also clear from the

dimensions of the respective problems - the QL eigenvalue problem is  $O(N_y \times N_y)$  whereas the corresponding CE2 problem is  $O(N_y^2 \times N_y^2)$  so it is clear there have to be  $O(N_y^2 - N_y)$  additional eigenvalues in  $\delta\text{CE2}$ .

Importantly, in Type A perturbations, it is clear that any additional instabilities in  $\delta\text{CE2}$  are dependent on the existence of an instability in  $\delta\text{QL}$  and are also always weaker (ie. their growth rates are smaller) than this QL instability. By exactly similar reasoning, there is also the possibility of additional unstable Type B perturbations in  $\delta\text{CE2}$ . However, here it is less straightforward to deduce their reliance on a QL instability being present or that this dominates their growth rates due to the mean flow perturbation feeding back onto the fluctuations equations. Nevertheless, this seems a plausible assumption: if it is not true, CE2 could exhibit a Type B bifurcation when QL does not.

In summary, the instability of the QL system is sufficient to conclude the same for the larger CE2 problem whereas concluding stability of CE2 given the stability of QL is true for Type A perturbations but remains a conjecture for Type B perturbations. With this one caveat, we adopt the stability of the smaller QL system as a proxy for the stability of the *much* larger CE2 system. We develop this crucial idea further in the next section.

### III. EXTENDED ORR-SOMMERFELD ANALYSIS

The  $\delta\text{QL}$  problem which includes some information on the second-order-flow statistics of the base flow will be called ‘Extended Orr-Sommerfeld’ stability analysis. We describe the approach as follows.

1. *Take the base flow ( $U, \mathbf{C}$ )*

This is assumed steady and so an instantaneous measurement is enough or, more likely, is time-averaged to make it so.

2. *Approximate each cumulant component tensor  $\mathbf{C}^{mn}$  as rank 1 to obtain a representative physical field  $\tilde{\mathbf{u}}_0^{mn}(\mathbf{y})$  for the wavenumber pairing  $(m, n)$  in the base state.*

While correlation matrices calculated directly from the instantaneous fluctuation fields of the flow are always of rank 1, time-averaging produces a higher rank matrix. A natural way to approximate the second order cumulant as rank 1 is by seeking  $\tilde{\mathbf{u}}_0^{mn}(\mathbf{y})$  that minimises the Frobenius matrix norm

$$\begin{aligned} \|\mathbf{C}^{mn} - \tilde{\mathbf{u}}_0^{mn} \otimes \tilde{\mathbf{u}}_0^{*mn}\|_F^2 &:= \sum_{i,j=1}^3 \sum_{p,q=1}^N (C_{i,j}^{mn}(p,q) - [\tilde{\mathbf{u}}_0^{mn}(\mathbf{y}_p)]_i [\tilde{\mathbf{u}}_0^{*mn}(\mathbf{y}_q)]_j) (C_{i,j}^{*mn}(p,q) - [\tilde{\mathbf{u}}_0^{*mn}(\mathbf{y}_p)]_i [\tilde{\mathbf{u}}_0^{mn}(\mathbf{y}_q)]_j) \\ &= \left\| \begin{pmatrix} C_{11}^{mn} & C_{12}^{mn} & C_{13}^{mn} \\ C_{21}^{mn} & C_{22}^{mn} & C_{23}^{mn} \\ C_{31}^{mn} & C_{32}^{mn} & C_{33}^{mn} \end{pmatrix} - \begin{bmatrix} \tilde{u}_{(1:N)}^{mn} \\ \tilde{v}_{(1:N)}^{mn} \\ \tilde{w}_{(1:N)}^{mn} \end{bmatrix} \begin{bmatrix} \tilde{u}_{(1:N)}^{*mn} & \tilde{v}_{(1:N)}^{*mn} & \tilde{w}_{(1:N)}^{*mn} \end{bmatrix} \right\|_F^2 \end{aligned} \quad (59)$$

where e.g.  $\tilde{u}_{(1:N)}^{mn} := [\tilde{u}^{mn}(\mathbf{y}_1) \tilde{u}^{mn}(\mathbf{y}_2) \cdots \tilde{u}^{mn}(\mathbf{y}_N)]^T$ . Since  $\mathbf{C}^{mn} = [\mathbf{C}^{mn}]^H$  (which is the Hermitian conjugate) and positive definite, the required  $\tilde{\mathbf{u}}_0^{mn}$  is the leading right eigenvector of  $\mathbf{C}^{mn}$  associated with the largest eigenvalue  $\sigma_1$  scaled so that  $|\tilde{\mathbf{u}}_0^{mn}| = \sqrt{\sigma_1}$ .

3. *Revert evolution equations for  $\mathbf{C}$  back to the equivalent Quasilinear (primitive) equations.*

This step is possible once a rank-1 approximation for each  $\mathbf{C}^{mn}$  is available

4. *Allow small perturbations in the mean,  $\delta U$ , and the fluctuation field,  $(\delta \tilde{\mathbf{u}}, \delta \tilde{p})$ .*

This step extends the standard approach by including the perturbations to the mean velocity profile  $\delta U$ .

5. *Examine the (extended) linear operator for  $(\delta U, \delta \tilde{\mathbf{u}}, \delta \tilde{p})$  to determine the nature of CE2 statistical stability.*

The resulting perturbation equations - the Extended Orr-Sommerfeld equations - are

$$\partial_t \delta U = \frac{1}{Re} \partial_y^2 \delta U + \delta G - \sum_{m,n} \partial_y (\delta \tilde{u}^{mn} \tilde{v}_0^{-m-n} + \tilde{u}_0^{mn} \delta \tilde{v}^{-m-n}) \quad (60)$$

and for each wavenumber pair  $(m, n)$

$$\partial_t \delta \tilde{\mathbf{u}}^{mn} = \frac{1}{Re} \nabla^2 \delta \tilde{\mathbf{u}}^{mn} - \nabla \delta \tilde{p}^{mn} - imU \delta \tilde{\mathbf{u}}^{mn} - \delta \tilde{v}^{mn} U_y \hat{\mathbf{x}} - im \delta U \tilde{\mathbf{u}}_0^{mn} - \tilde{v}_0^{mn} \delta U_y \hat{\mathbf{x}} \quad (61)$$

$$im \tilde{u}^{mn} + \partial_y \tilde{v}^{mn} + in \tilde{w}^{mn} = 0 \quad (62)$$

(coloured terms depend on  $\delta U$  to be discussed later). Now the eigenvalue problem has size  $(N_y + 4N_x N_y N_z)^2 \approx 16N_x^2 N_y^2 N_z^2$  which is impractical for all but the smallest systems since all the wavenumber pairings are coupled through the mean equation. A natural way to simplify the calculation is to only include a targetted subset of the wavenumber pairings and, going further, to only consider one wavenumber pairing. This latter approximation is obviously the most extreme but is also closest in spirit to the original Orr-Sommerfeld analysis - we call this ‘minimally Extended Orr-Sommerfeld’ (mEOS) analysis.

#### A. minimally Extended Orr-Sommerfeld equations (mEOS)

Here, the sum over wavenumber pairings in (A.3) is removed leaving

$$\partial_t \delta U = \frac{1}{Re} \partial_y^2 \delta U + \delta G - \partial_y (\delta \tilde{u}^{mn} \tilde{v}_0^{-m-n} + \tilde{u}_0^{mn} \delta \tilde{v}^{-m-n} + c.c.) \quad (63)$$

with

$$\partial_t \delta \tilde{\mathbf{u}}^{mn} = \frac{1}{Re} \nabla^2 \delta \tilde{\mathbf{u}}^{mn} - \nabla \delta \tilde{p}^{mn} - imU \delta \tilde{\mathbf{u}}^{mn} - \delta \tilde{v}^{mn} U_y \hat{\mathbf{x}} - im \delta U \tilde{\mathbf{u}}_0^{mn} - \tilde{v}_0^{mn} \delta U_y \hat{\mathbf{x}} \quad (64)$$

$$im \tilde{u}^{mn} + \partial_y \tilde{v}^{mn} + in \tilde{w}^{mn} = 0 \quad (65)$$

The eigenvalue problem size is now  $(5 \times N_y)^2 = 25N_y^2$  but potentially needs to be repeated for all wavenumber pairings of interest. This workload is now comparable to OS analysis.

#### B. Infinitely-Extended Orr-Sommerfeld equations (iEOS)

Before going on to test EOS and mEOS on some flows, it’s worth briefly discussing how far this approach of using the cumulant framework to further motivate more sophisticated versions of Orr-Sommerfeld analysis can go. In fact, it turns out that only one further enhancement is possible and then only for  $CE_\infty$ . This is because any intermediate closure will lead to an equation which when ‘unwrapped’ at the highest level contradicts those obtained at lower cumulant orders. To see this, consider CE3, the next closure after CE2 in which  $\mathbf{C}^{(4)}$  is ignored. Unwrapping the statistical equation for  $\mathbf{C}$  will recover the Navier-Stokes equations whereas unravelling the  $\mathbf{C}^{(3)}$  equations will not as the nonlinear term leading to  $\mathbf{C}^{(4)}$  has been dropped (any other closure will also suffer this inconsistency). The only way to avoid this is: 1) to only unwrap one cumulant equation - so CE2 which leads to EOS, or 2) ensure that all unwrapped equations are the same which means no closure and  $CE_\infty$ . In this latter case, the Navier-Stokes equations re-emerge which, under perturbation around a steady base state, lead to the linearized Navier-Stokes equations as the ultimate extension of OS analysis, i.e.

$$\partial_t \delta U = \frac{1}{Re} \partial_y^2 \delta U + \delta G - \sum_{m,n} \partial_y (\delta \tilde{u}^{mn} \tilde{v}_0^{-m-n} + \tilde{u}_0^{mn} \delta \tilde{v}^{-m-n}) \quad (66)$$

and for each wavenumber pair  $(m, n)$

$$\partial_t \delta \tilde{\mathbf{u}}^{mn} = \frac{1}{Re} \nabla^2 \delta \tilde{\mathbf{u}}^{mn} - \nabla \delta \tilde{p}^{mn} - imU \delta \tilde{\mathbf{u}}^{mn} - \delta \tilde{v}^{mn} U_y \hat{\mathbf{x}} - im \delta U \tilde{\mathbf{u}}_0^{mn} - \tilde{v}_0^{mn} \delta U_y \hat{\mathbf{x}} \quad (67)$$

$$-[\delta \tilde{\mathbf{u}} \cdot \nabla \tilde{\mathbf{u}}_0 + \tilde{\mathbf{u}}_0 \cdot \nabla \delta \tilde{\mathbf{u}}]^{mn} \quad (68)$$

$$im \tilde{u}^{mn} + \partial_y \tilde{v}^{mn} + in \tilde{w}^{mn} = 0$$

This could be called an ‘Infinitely-Extended Orr-Sommerfeld’ problem (or iEOS for short) as there is no further extension possible with the cumulant expansion framework considered here. It’s worth remarking that the extra term added in iEOS would get dropped in any minimal version where the individual wavenumber pairings are considered separately: i.e. minimizing iEOS is just mEOS. There is, however, considerable potential in avoiding this drastic reduction in favour of retaining small subsets of interacting wavenumber pairings such as triads which interact through the newly present term. This or iEOS will not be pursued further here to avoid overcomplicating the discussion.

### IV. APPLICATION

We now test the extended stability approaches, EOS and mEOS, upon statistically-steady states obtained by direct numerical simulations of 2D channel flow. The simulations are performed using the open-source partial differential equation solver Dedalus

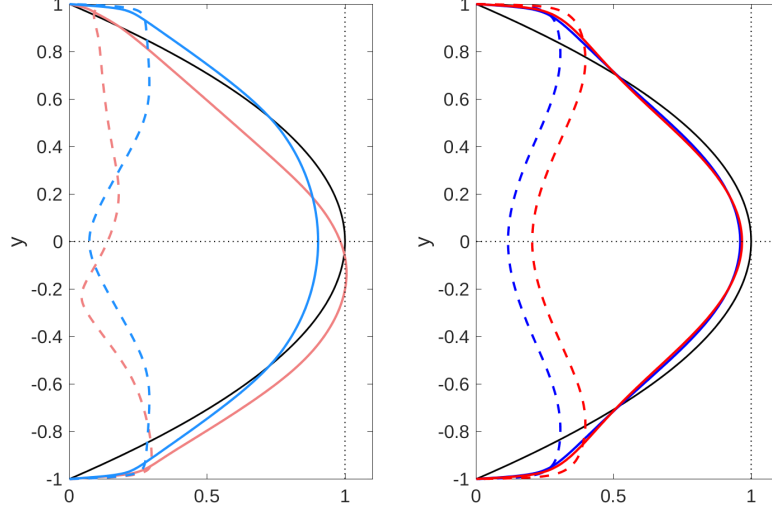


FIG. 2: Mean velocity profiles (solid lines) and streamwise root-mean-squared velocity profiles (dashed lines) for the four 2D channel test states at  $Re = 36,300$ . Left: states with an applied pressure gradient: symmetric S (light blue) and asymmetric A (pink). Right: body forced states F1 (blue) and F2 (red). Black solid line shows the laminar parabolic profile in both plots for reference.

[67]. The 2D flow is simulated using a vorticity-streamfunction formulation so that  $(u, v) := (\psi_y, -\psi_x)$  and

$$\omega_t + \psi_y \omega_x - \psi_x \omega_y = \frac{1}{Re} \nabla^2 \omega - \partial_y f(y, t), \quad \omega := -\nabla^2 \psi \quad (69)$$

where the flow is driven by a streamwise body force  $f(y, t)\hat{\mathbf{x}}$  so that the volume flux is fixed.  $Re$  is defined as in §II A so the following conditions are imposed

$$\psi(-1) = 0, \quad \psi(1) = \frac{4}{3}, \quad \psi_y(-1) = 0, \quad \psi_y(1) = 0. \quad (70)$$

with the latter two reflecting the presence of non-slip walls. Following earlier work [60, 68], the length of the channel is set to 4 times its height ( $L_x = 4$ ),  $Re = 36,300$  and computationally, 1024 Fourier modes are used to discretize in the  $x$  direction and 256 Chebyshev modes in  $y$  (see [60] for details).

The streamwise body force is defined in terms of a profile function  $g(y)$  as follows

$$f(y, t) := G(t)(g(y) - 1) \quad (71)$$

where setting  $g = 0$  recovers the usual  $y$ -independent applied pressure gradient  $-G(t)$ . For this situation it is already known that there is bistability with two statistically steady states possible in 2D channel flow at  $Re = 36,300$  [60]: a state which is statistically symmetric about the channel midplane - the symmetric state S - and another which is statistically asymmetric - the asymmetric state A: see Fig. 2(left). Choosing non-zero  $g(y)$  is a device to diversify the test states available with two extra examples generated by using profiles  $g_1 := (1 - y^2)^6$  (state F1) and  $g_2 := \cos \frac{3}{2}\pi y^2$  (state F2).

### A. Statistically stable test states

The mean profiles for states S, A, F1 and F2 are shown in Fig. 2 along with their streamwise root-mean-squared velocity profiles, all obtained by time-averaging over  $10^4$  time units. Their respective power spectra are shown in Fig. 3 (left). While the dominant wavenumber is the same for all four states ( $k_d = 2\alpha = \pi/2$ ), significant differences are seen at neighbouring streamwise wavenumbers  $2k_d$  and  $3k_d$  for example. Typical temporal variations of the fluctuation field energy  $E_{fluct}$  compared to the total energy of the flow  $E$  - Fig. 3 (right) - show the desired wide variety of mean fluctuation energy and fluctuation amplitudes. In particular, the amplitude of the fluctuations in state F2 are  $\approx 60\%$  of the mean and only  $\approx 30\%$  for state A.

For each state the second-order cumulant matrices were computed every unit of time and then averaged over a period of  $10^3$ . During the process of calculating EOS and mEOS eigenvalues, correlation matrices time-averaged over different time windows



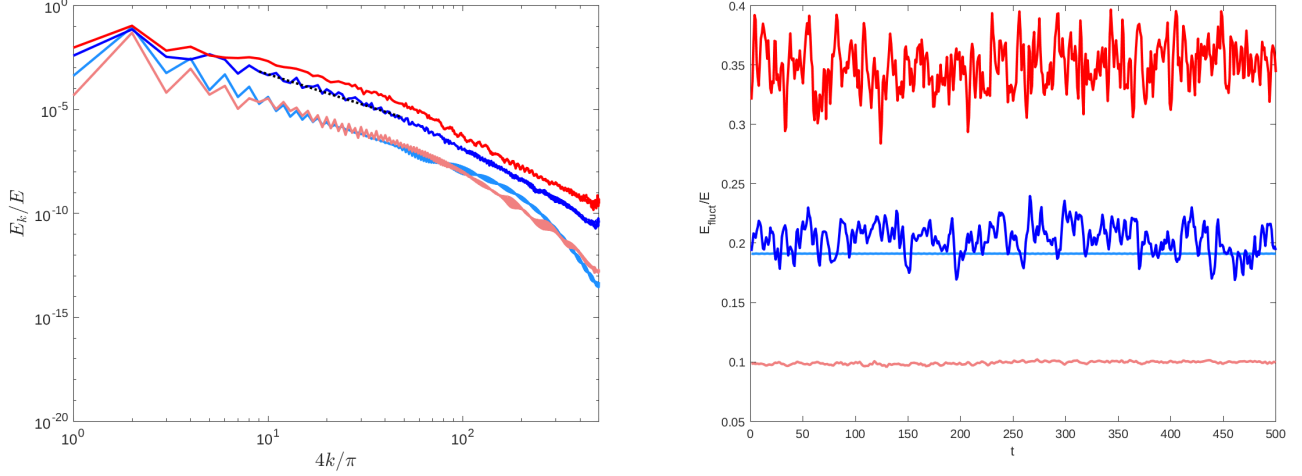


FIG. 3: Fluctuation energy as a ratio to the total flow energy for the four 2D channel test states at  $Re = 36,300$ : symmetric S (light blue), asymmetric A (pink), F1 (blue) and F2 (red). Left: decomposition by streamwise wavenumber  $k$ , right: temporal fluctuations over a typical time-averaging window.

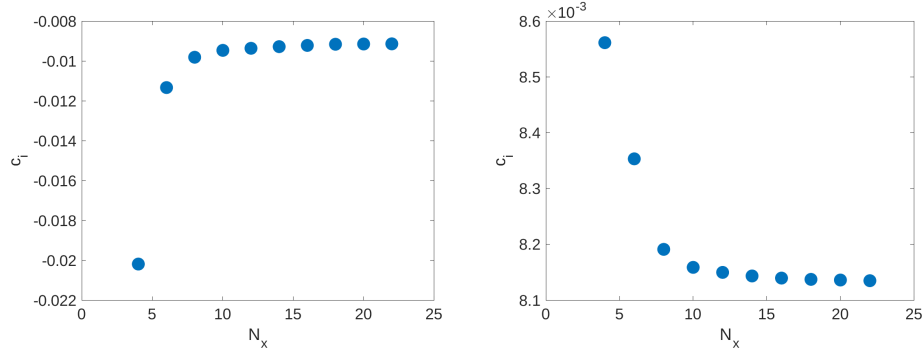


FIG. 4: Typical eigenvalue convergence with respect to the total number of the streamwise wavenumbers  $N_x$  included in the EOS model, shown for  $k = 2$  (left) and  $k = 3$  (right) for the F2 state.

$t = 500, 1000, 1500$  were used as well as correlation matrices time-averaged with different time-steps (0.5 and 1) for one time window  $t=500$ . The qualitative results were all the same, with only minor quantitative differences which did not affect the relative positions of eigenvalues obtained by different methods. The time-averaged cumulant matrix was then diagonalised and the flow field corresponding to the leading (real) eigenvalue used to typify the base fluctuation field. The implications of the time-averaging to the rank of the matrix are discussed in §V A.

The EOS problem - equations (A.3)-(A.9) - and the mEOS problem - equations (63)-(65) - were posed as generalised matrix eigenvalue problems of matrix size  $\approx (4N_x N_y)^2$  and  $(5N_y)^2$  respectively. For EOS,  $N_x = 20$  streamwise wavenumbers were used as it provides a balance between accurate eigenvalue convergence and computational accessibility: e.g. see Fig. 4. Wall-normal resolution of the eigenvalue problem was also varied to ensure eigenvalue convergence in the mEOS case. Doubling the wall-normal resolution from the DNS resolution of 256 Chebyshev modes to 512 produced less than a  $10^{-8}$  relative error in the eigenvalues so all stability calculations were done using the DNS wall-normal resolution.

## B. Comparisons

Here we compare the eigenvalues obtained by standard (OS), extended (EOS) and minimally extended Orr-Sommerfeld (mEOS) stability analyses on the four different turbulent states. Since all our test cases are statistically steady, for a model to be good at predicting statistical stability of the turbulent state, we expect all the eigenvalues to be stable, i.e. to have a negative real part. For the symmetric (top left, figure 5) and asymmetric (top right, figure 5) states, we observe no significant difference in the

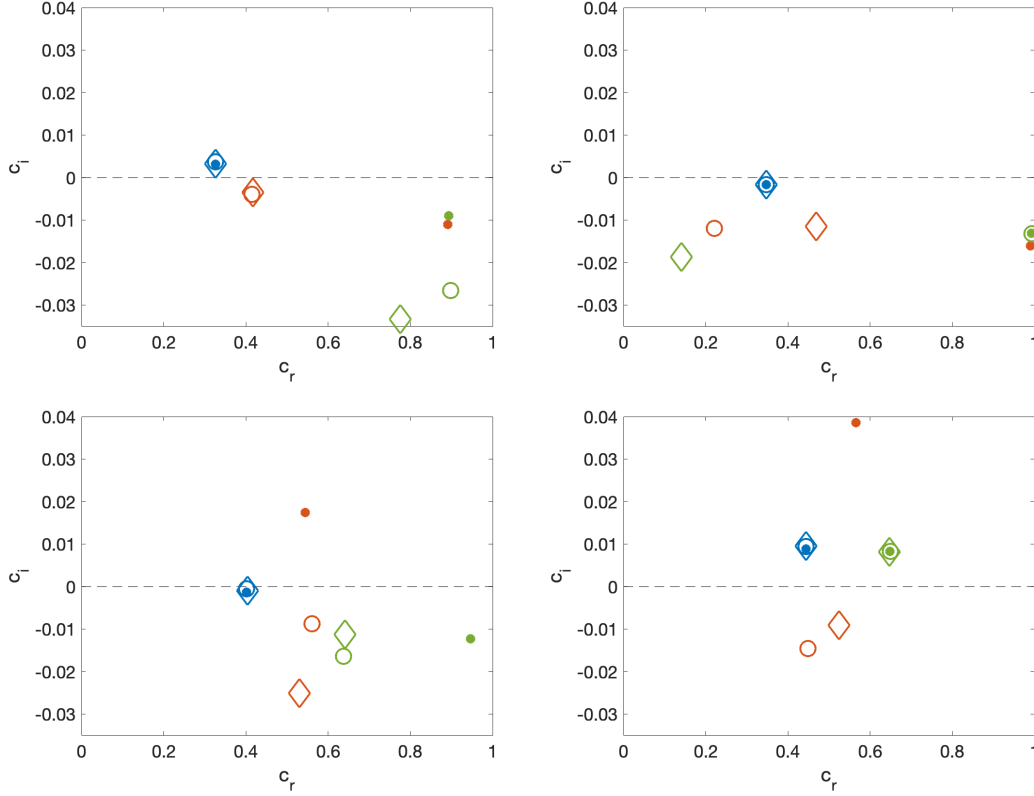


FIG. 5: Comparison of the eigenvalues  $\sigma = -im\alpha(c_r + ic_i)$  - so growth rate is  $m\alpha c_i$  - for OS ( $\bullet$ ), EOS ( $\diamond$ ) and mEOS analysis ( $\circ$ ). Only the leading eigenvalues for  $m = 1$  (blue),  $m = 2$  (red) and  $m = 3$  (green) are shown. Top left: symmetric S, top right: asymmetric A, bottom left: F1, bottom right: F2 states.

leading eigenvalues between the three stability models. While all three models predict the asymmetric state to be statistically stable, they also all predict statistical instability for the symmetric state. For these test states, the leading eigenvalue is associated with the first streamwise wavenumber (marked blue in the plot). We observe some changes for the other eigenvalues which we do not examine further as they are all stable and do not affect characterization of statistical stability of the turbulent states.

Since all streamwise wavenumbers are coupled in the extended model, the leading wavenumber for the eigenvalue is assigned by examining the power spectrum of the corresponding eigenvector. Example power spectra for leading eigenvalues are shown in figure 6 where it is apparent that the mean velocity component of an eigenvector is at least an order of magnitude smaller than the leading wavenumber contribution.

The leading eigenvalue for the body-forced states states F1 (bottom left, figure 5) and F2 (bottom right, figure 5) is associated with the second streamwise wavenumber (marked red in the plot). For both F1 and F2 states, this eigenvalue is unstable in the standard stability analysis but becomes stable in EOS. The stabilisation effect is also captured by mEOS but isn't so strong. While the statistical stability of the F1 state is predicted correctly by the extended model, the improvement is only partial for the F2 state. In addition to the unstable leading eigenvalue which is stabilised by the extended model, there are two subsequent unstable eigenvalues corresponding to the first and third streamwise wavenumbers (marked blue and green on the plot). Similar to the symmetric state case, these two unstable eigenvalues see no improvement towards stability when the extended stability models are applied.

So, in summary, for each unstable eigenvalue observed in our test cases, the standard and extended models either agree on their statistical stability prediction, or the extended model shifts the prediction towards statistical stability. The stabilising effect is qualitatively captured by both EOS and mEOS with the mean velocity components making a non-zero power contribution to the eigenvectors of the extended model. We now examine why the extended stability models sometimes perform better than OS and sometimes make very little improvement.

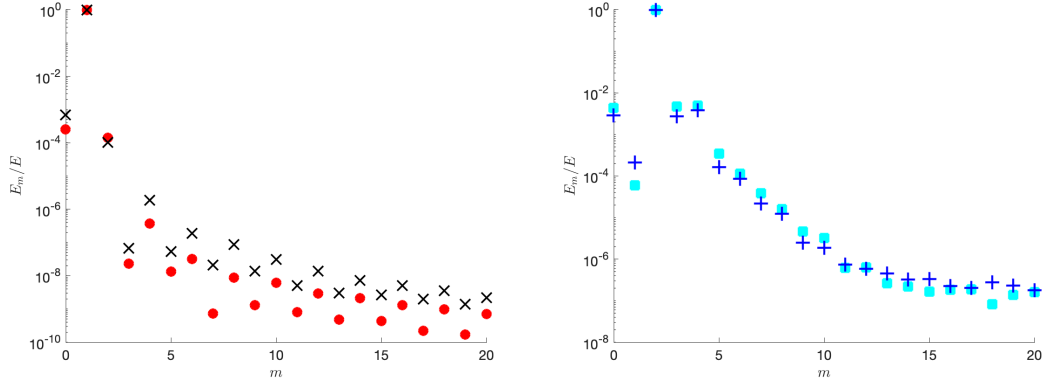


FIG. 6: Power spectra for the EOS eigenvectors for the leading eigenvalues. Left: symmetric S state ( $\times$ ) and asymmetric A state ( $\bullet$ ) with  $m = 1$ ; Right: states F1 ( $\blacksquare$ ) and F2 ( $+$ ) with  $m = 2$ . The mean velocity perturbation ( $m = 0$ ) is at least an order of magnitude smaller than the leading wavenumber contribution to the power spectrum in all 4 cases.

F2 state: leading eigenvalue for $m = 2$		S state: leading eigenvalue for $m = 1$	
$\sigma_{OS}$	$0.06058 + 0.8888i$	$\sigma_{OS}$	$0.0024849 + 0.25601i$
$\sigma_{OS} + \Delta\sigma_A + \Delta\sigma_S$	$-0.16937 + 0.80087i$	$\sigma_{OS} + \Delta\sigma_A + \Delta\sigma_S$	$0.0029878 + 0.25637i$
$\sigma_{mEOS}$	$-0.02294 + 0.7043i$	$\sigma_{mEOS}$	$0.0028772 + 0.25653i$
$\Delta\sigma_A$	$0.02738 + 0.05860i$	$\Delta\sigma_A$	$0.00011499 - 0.0000561i$
$\Delta\sigma_S$	$-0.25733 - 0.02933i$	$\Delta\sigma_S$	$0.00038787 + 0.0004194i$

TABLE I: Perturbation analysis results for the leading eigenvalue in the F2 state (left) and the symmetric S state (right). The first order change in the eigenvalue caused by the advection ( $\Delta\sigma_A$ ) and shear ( $\Delta\sigma_S$ ) are shown in the minimal extended Orr-Sommerfeld model (mEOS). Unperturbed (standard Orr-Sommerfeld) eigenvalues are given by  $\sigma_{OS}$  and mEOS eigenvalues are given by  $\sigma_{mEOS}$ . The Table shows that F2 changes to being stable when using mEOS whereas S remains unstable.

### C. Eigenvalue perturbation analysis

The logical first approach to rationalising the improvement (stabilisation) or not in mEOS of the leading eigenvalues is to carry out an eigenvalue perturbation analysis. While this neglects the interactions between different streamwise wavenumbers, it includes the minimal improvement that our models offer: adding the mean velocity perturbation into the stability consideration. This leads to an additional equation which governs the evolution of the mean velocity perturbation, and two extra terms - advection and shear - which affect the fluctuation perturbations. While formally limited to only small effects, the perturbation analysis provides a framework to study the structures of the mean velocity perturbations, base fluctuations and fluctuation perturbations and how their interactions affect the eigenvalues.

The unperturbed mEOS eigenvalue problem is the OS problem (equation (65) without the  $\delta U$  coloured terms) and (63) (we are imagining a small number  $\varepsilon$  inserted in front of the coloured terms and developing a perturbation expansion in this but actually  $\varepsilon = 1$ ). The latter is passive: it sets  $\delta U$  but there is no feedback to the OS equation. Discretized, it reads

$$A\mathbf{y}_R = \sigma B\mathbf{y}_R \quad (72)$$

with matrices  $A, B$ , eigenvalue  $\sigma$  and right eigenvector  $\mathbf{y}_R := [\delta U \delta \tilde{\mathbf{u}}^{m0}]^T$ . The coloured  $\delta U$  terms in (65) are then treated as perturbations of  $A$  which causes  $(\sigma, \mathbf{y}_R) \rightarrow (\sigma + \Delta\sigma, \mathbf{y}_R + \Delta\mathbf{y}_R)$  so that

$$(A + \delta A_A + \delta A_S)(\mathbf{y}_R + \delta \mathbf{y}_R) = (\sigma + \delta\sigma)B(\mathbf{y}_R + \delta \mathbf{y}_R) \quad (73)$$

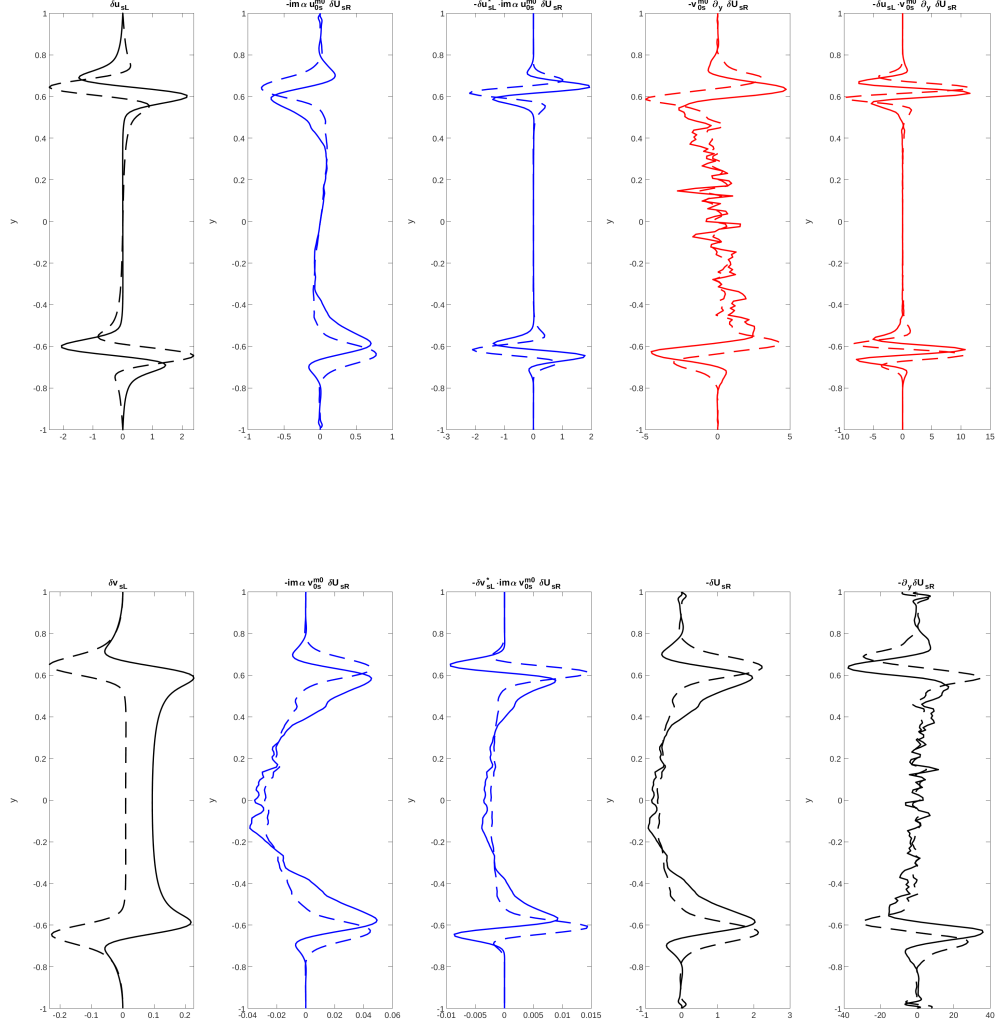


FIG. 7: Perturbation analysis results for F2 state. Top row: streamwise component of the unperturbed left eigenvector  $\delta u_{sL}$ , streamwise component of the perturbed advection term  $-im\alpha u_{0s}^{m0} \delta U_{sR}$  and the product of the two  $-\delta u_{sL}^* \cdot im\alpha u_{0s}^{m0} \delta U_{sR}$ , streamwise component of the perturbed shear term  $-v_{0s}^{m0} \partial_y \delta U_{sR}$  and the product of the left eigenvector and the shear term  $-\delta u_{sL}^* \cdot v_{0s}^{m0} \partial_y \delta U_{sR}$ . Bottom row: wall-normal component of the unperturbed left eigenvector  $\delta v_{sL}$ , wall-normal component of the perturbed advection term  $-im\alpha v_{0s}^{m0} \delta U_{sR}$  and the product of the two  $-\delta v_{sL}^* \cdot im\alpha v_{0s}^{m0} \delta U_{sR}$ , mean profile component of the unperturbed right eigenvector  $-\delta U_{sR}$  and its  $y$ -derivative  $-\partial_y \delta U_{sR}$ . Solid (dashed) lines indicate real (imaginary) parts of the vectors. Subscript  $(\cdot)_s$  refers to the sine components of the eigenfunctions as explained in the Appendix.

where  $\delta A_A \mathbf{y}_R$  corresponds to the advection term  $-im\alpha \tilde{\mathbf{u}}_0^{m0} \delta U_R$  and  $\delta A_S \mathbf{y}_R$  to the shear term  $-\tilde{v}_0^{m0} \partial_y \delta U_R \hat{\mathbf{x}}$ . By taking the inner product using the left eigenvector of the unperturbed system  $\mathbf{y}_L$ , and considering first order terms only, an expression then follows for the first order perturbation to the eigenvalue  $\delta\sigma$ :

$$\delta\sigma = \delta\sigma_A + \delta\sigma_S := \frac{\mathbf{y}_L^\dagger \delta A_A \mathbf{y}_R}{\mathbf{y}_L^\dagger B \mathbf{y}_R} + \frac{\mathbf{y}_L^\dagger \delta A_S \mathbf{y}_R}{\mathbf{y}_L^\dagger B \mathbf{y}_R} \quad (74)$$

We present the two most interesting cases of the eigenvalue perturbation analysis. In the first case, we perform eigenvalue perturbation analysis on the leading eigenvalue of the standard Orr-Sommerfeld analysis for the F2 state, which is seen to stabilise

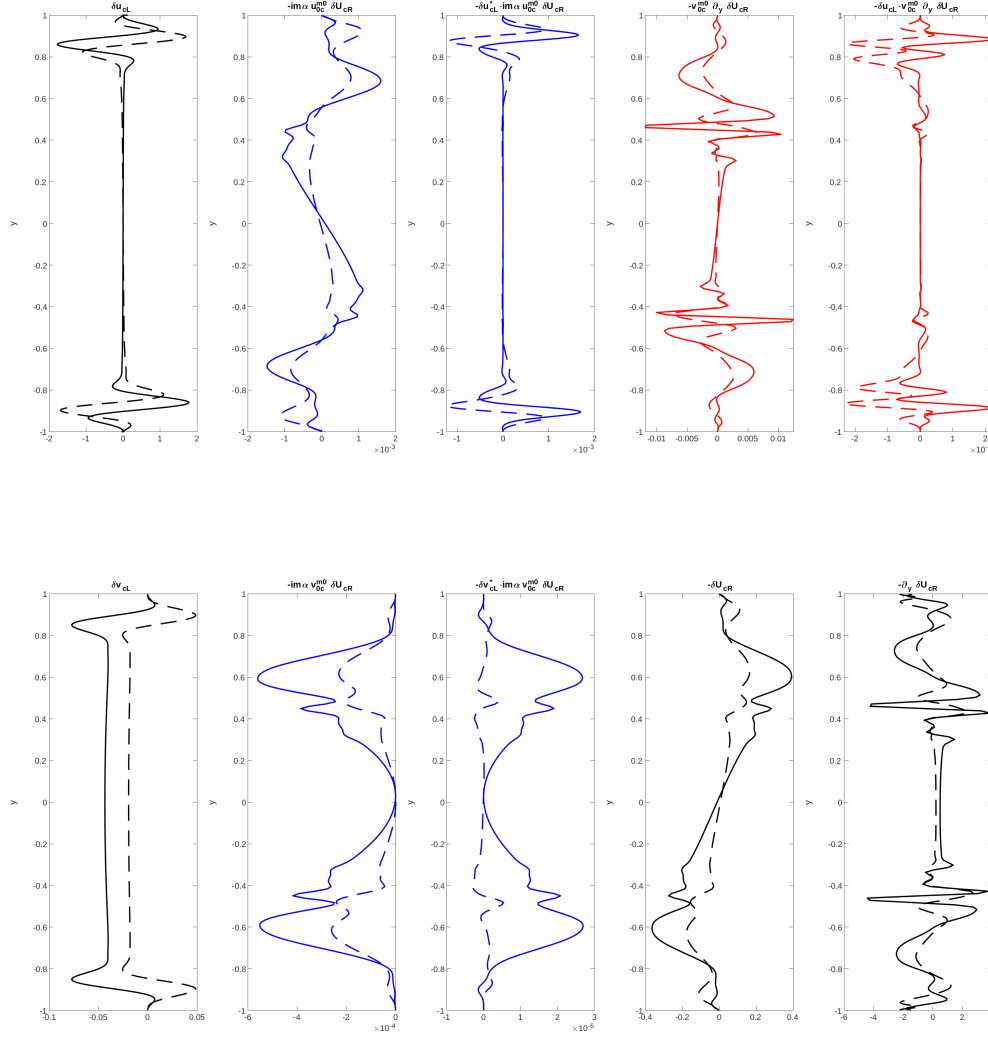


FIG. 8: Perturbation analysis results for S state. Top row: streamwise component of the unperturbed left eigenvector  $\delta u_{cL}$ , streamwise component of the perturbed advection term  $-im\alpha v_{0c}^{m0} \delta U_{cR}$  and the product of the two  $-\delta u_{cL}^* \cdot im\alpha v_{0c}^{m0} \delta U_{cR}$ , streamwise component of the perturbed shear term  $-v_{0c}^{m0} \partial_y \delta U_{cR}$  and the product of the left eigenvector and the shear term  $-\delta u_{cL}^* \cdot v_{0c}^{m0} \partial_y \delta U_{cR}$ . Bottom row: wall-normal component of the unperturbed left eigenvector  $\delta v_{cL}$ , wall-normal component of the perturbed advection term  $-im\alpha v_{0c}^{m0} \delta U_{cR}$  and the product of the two  $-\delta v_{cL}^* \cdot im\alpha v_{0c}^{m0} \delta U_{cR}$ , mean profile component of the unperturbed right eigenvector  $-\delta U_{cR}$  and its  $y$ -derivative  $-\partial_y \delta U_{cR}$ . Solid (dashed) lines indicate real (imaginary) parts of the vectors. Subscript  $(\cdot)_c$  refers to the cosine components of the eigenfunctions as explained in the Appendix.

in mEOS and EOS. The second case corresponds to the leading eigenvalue of the symmetric state, which shows no significant difference between the standard and extended approaches. The eigenvalues as well as perturbation analysis predictions are summarised in Table I. The left and right eigenvectors and perturbed terms are shown in figures 7 and 8.

For the body-force-driven F2 case, the advection term has a small and positive contribution to the real part of  $\delta\sigma$  while the shear term has a large negative contribution to the real part of  $\delta\sigma$ , as summarised in Table 1. This latter prediction is only qualitatively correct as the shear term is not a small perturbation giving a much larger predicted decay rate of  $-0.169$  than the actual value of  $-0.023$  obtained from mEOS. The perturbation analysis, however, indicates that the shear in the perturbed mean field is causing the stabilisation. Looking in more detail at the fields in figure 7, it is clear that the active regions of the left and right eigenvectors

coincide. In particular, the shear in  $\delta U_R$  coincides with where the left eigenvector is significant and is of opposite phase giving the large stabilising effect. In contrast, the resulting advection term is not only an order of magnitude smaller than the shear term, but also has the same sign contribution as the left eigenvector, yielding a small destabilizing contribution to the eigenvalue.

For the symmetric S case, the perturbation analysis shows both advection and shear terms make small destabilizing contributions to the eigenvalue commensurate with mEOS although there is still an error due to the finiteness of the perturbation. Examining the structure of the left and right eigenvectors shown in figure 8 indicates that they are ill-matched. The left eigenvector is concentrated much closer to the channel walls than the right eigenvector. Moreover, even though the right eigenvector component  $\delta U$  has some structure near the wall, the interaction of this component with the perturbed operators moves this structure towards the centre of the wall for the shear term, avoiding any significant interaction with the left eigenvector. The advection term has some overlap with the left eigenvector, but it is also an order of magnitude smaller than the shear term, overall resulting in small destabilizing contributions. It's also worth remarking that even at resolution of 2048 wall-normal Chebyshev modes, the eigenvectors possess the same small scale structure seen in the figures.

The ‘take home’ message from this section is that the mean velocity perturbation, even if an order magnitude smaller than the other components of the eigenvector - see Figure 6, can interact with the base flow fluctuation fields in a way that produces a strong stabilising influence.

## V. MODEL LIMITATIONS

In this section, we discuss the various approximations made in deriving EOS and mEOS which include time-averaging the statistics, approximating correlation matrices as rank 1 and neglecting higher order statistics.

### A. Rank 1 approximation of correlation matrices

Time-averaging the correlation matrix increases its rank from 1 up to potentially its full dimension - see Fig. 9 for singular values  $\sigma_i$  of correlation matrices time-averaged over 1000 time units. For  $m = 2$  which is the dominant streamwise wave-number in all of the test states, a gap between the leading and the second singular values is larger than an order of magnitude indicating that a rank-1 approximation of the time-averaged correlation matrix may be reasonable. On another hand, time-averaged correlation matrices for  $m \in \{1, 3\}$  do not show a significant gap between the leading and second singular values. In this case, it is much more likely that some important fluctuation field features might not be accurately represented by the rank 1 representation of the correlation matrix and, as a result, the approach is less justified.

In an attempt to explore a more accurate representation of  $\mathbf{C}^{mn} = \sum_{i=1} \sigma_i \hat{\mathbf{e}}_i \otimes \hat{\mathbf{e}}_i$  (where  $\hat{\mathbf{e}}_i$  is the  $i^{\text{th}}$  normalised eigenvector and  $\sigma_i$  the largest eigenvalue or singular value of  $\mathbf{C}^{mn}$  as it is Hermitian) beyond just the rank-1 approximation  $\mathbf{C}^{mn} \approx \sigma_1 \hat{\mathbf{e}}_1 \otimes \hat{\mathbf{e}}_1$  ( $\tilde{\mathbf{u}}_0^{mn} = \sqrt{\sigma_1} \hat{\mathbf{e}}_1$ ), a weighted average of the leading  $N$  fields,

$$\tilde{\mathbf{u}}_0^{mn} = \sum_{i=1}^N \frac{\sigma_i}{\sum_{i=1}^N \sigma_i} \sqrt{\sigma_i} \hat{\mathbf{e}}_i, \quad (75)$$

was also considered for the F2 state where both  $m = 1$  and  $m = 2$  wavenumbers have a non-rank 1 time-averaged correlation matrix  $\mathbf{C}^{m0}$ . However, including  $N = 1, 2, 5$  or even 10 eigenvectors into the expansion showed no significant difference in the leading eigenvalues (less than 1% difference in the absolute value of the eigenvalue). Understanding the effect of a rank-1 approximation really requires time-stepping the full statistical equations which is beyond the scope of this work.

### B. Time-averaged statistics

To understand the effect of time-averaging the statistics in the Extended Orr-Sommerfeld stability models, numerical experiments were performed in which the perturbations to the turbulent base flow were exposed to a time-varying base flow. This experiment was first performed for the symmetric (S) state where the unstable Orr-Sommerfeld eigenvalue remains unstable in EOS and mEOS. From the DNS data, 10 turbulent flow histories were taken of length  $\Delta t = 500$  separated by at least 1000 time units to avoid statistical dependence. Each was taken as a turbulent, time-dependent base flow. Two random perturbations with energy  $E_{\text{pert}} = 10^{-5} E_{\text{base}}$  of the base flow were then added to each of the 10 base flow histories (making a total of 20 cases) and then their evolution computed over a  $\Delta t = 500$  time window using the QL equations. For  $(\delta U, \delta \tilde{\mathbf{u}}^{m0})$ , these read

$$\partial_t \delta U = \frac{1}{Re} \partial_y^2 \delta U + \delta G - [\tilde{\mathbf{u}}_0(t) \cdot \nabla \delta \tilde{\mathbf{u}} + \delta \tilde{\mathbf{u}} \cdot \nabla \tilde{\mathbf{u}}_0(t)]^{00} \quad (76)$$

$$\partial_t \delta \tilde{\mathbf{u}}^{m0} = \frac{1}{Re} \nabla^2 \delta \tilde{\mathbf{u}}^{m0} - \nabla \delta \tilde{p}^{m0} - imU \delta \tilde{\mathbf{u}}^{m0} - \delta \tilde{v}^{m0} U_y \hat{\mathbf{x}} - im \delta U \tilde{\mathbf{u}}_0^{m0} - \tilde{v}_0^{m0} \delta U_y \hat{\mathbf{x}}, \quad m > 0 \quad (77)$$

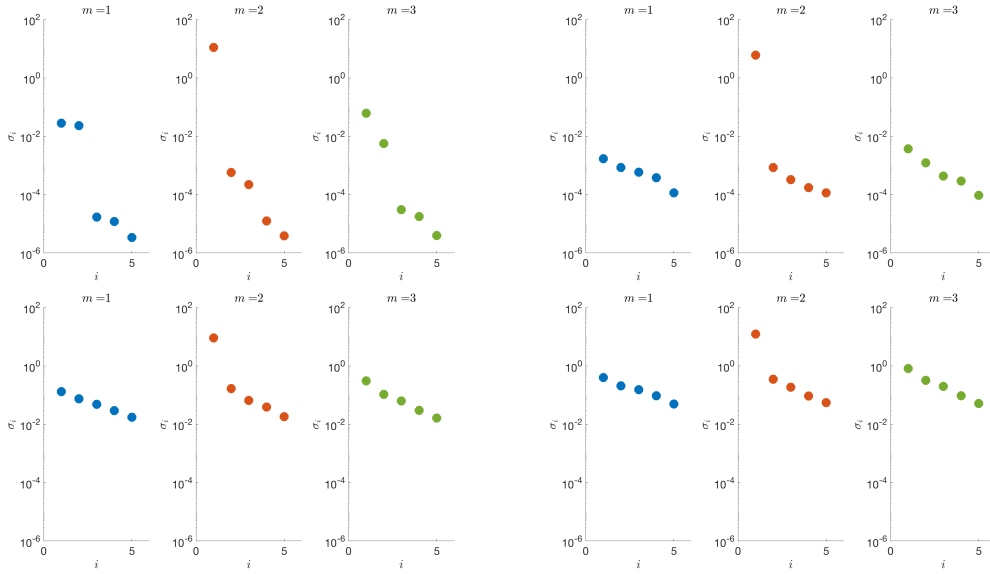


FIG. 9: Leading singular values  $\sigma_i$  of the correlation matrices  $\mathbf{C}^{m0}$  time-averaged over 1000 time units. Shown for  $m = 1$  (blue),  $m = 2$  (red) and  $m = 3$  (green). Top left: symmetric S, top right: asymmetric A, bottom left: F1, bottom right: F2 states. Note the gap after the leading singular value for  $m = 2$  (red) across all states confirming rank 1 approximation of the correlation matrix for the cases when mEOS and EOS analyses show stabilisation.

so that the perturbation-base flow fluctuation interactions are not included in the perturbation fluctuation equation (compare with (78) below where they are retained). Averaging the perturbation energy growth over the 20 different simulations revealed an unstable mode with exponential growth after initial transients decayed. The growth rate of this unstable mode was found to be  $\sigma = 0.00263$  which is within 5% of the growth rate predicted by the Extended Orr-Sommerfeld analysis - see Fig. 10. The most unstable eigenvectors of the EOS and mEOS analyses agree and are observed as the growing structure in this QL experiment - see Fig. 11. We conclude that time dependence of the base flow is not enough to recover the statistical stability of the symmetric state S.

### C. Importance of higher order statistics

To evaluate the need of flow statistics beyond the second order to recover statistical stability of the symmetric (S) state, we repeated the numerical experiment described above but this time the perturbation fields were time-stepped using the linearised Navier-Stokes equations where perturbation-base flow fluctuation interactions are now included and the base flow is time varying: viz.

$$\partial_t \delta \tilde{\mathbf{u}}^{m0} = \frac{1}{Re} \nabla^2 \delta \tilde{\mathbf{u}}^{m0} - \nabla \delta \tilde{p}^{m0} - imU(t) \delta \tilde{\mathbf{u}}^{m0} - \delta \tilde{v}^{m0} U_y(t) \hat{x} - im \delta U \tilde{\mathbf{u}}_0^{m0}(t) - \tilde{v}_0^{m0}(t) \delta U_y \hat{x} - [\tilde{\mathbf{u}}_0(t) \cdot \nabla \delta \tilde{\mathbf{u}} + \delta \tilde{\mathbf{u}} \cdot \nabla \tilde{\mathbf{u}}_0(t)]^{m0}. \quad (78)$$

We repeat the experiment with initial  $E_{pert} = 10^{-5} E_{base}$  and  $E_{pert} = 10^{-7} E_{base}$  obtaining the same qualitative results. When the energy growth of the perturbation field is time-averaged over 20 different runs, the perturbation growth is seen to saturate after an initial transient growth - see Fig. 10 (top). This suggests that the higher order statistics ignored in QL are important here for recovering statistical stability of the symmetric (S) turbulent state.

### D. Non-linear effects

Extended Orr-Sommerfeld stability analysis applied to the body force F2 state shows a significant stabilisation of the eigenvalue corresponding to the second streamwise wavenumber, but shows no significant difference for the other two unstable eigenvalues of the standard Orr-Sommerfeld approach. Repeating the numerical experiments described above applied to the F2 state shows that both the quasi-linear (QL) equations *and* the linearised Navier-Stokes (LNS) equations yield rapid exponential growth of the perturbations applied to the time-dependent base flow: see Figure 10 (bottom). Periodically renormalising the growing perturbation in the latter LNS case and continuing the simulation shows sustained growth over a period of  $O(1000)$

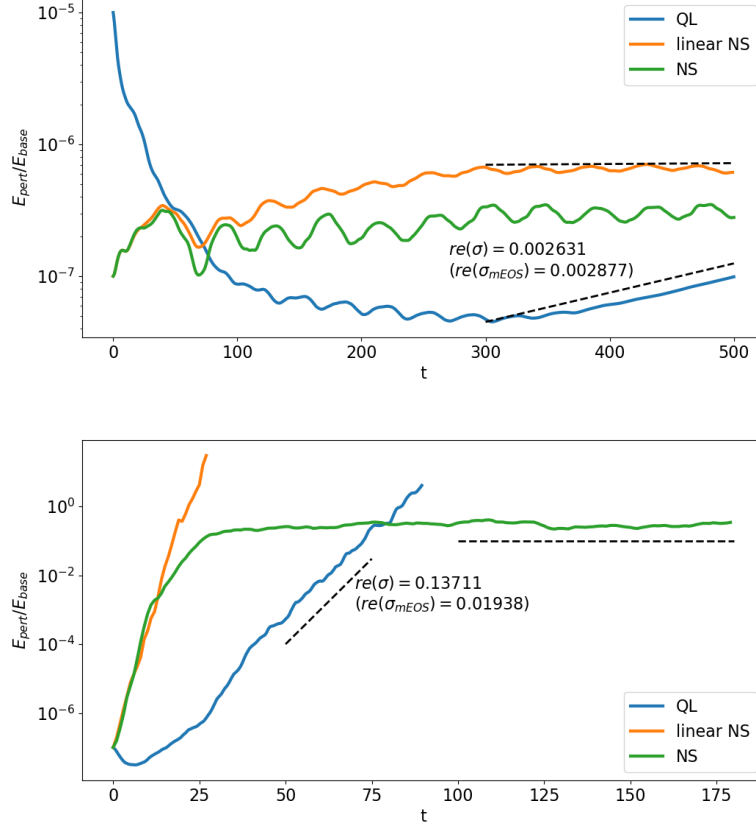


FIG. 10: Results of various numerical experiments: time evolution of the perturbation energy  $E_{pert}$  as a ratio to the base flow energy  $E_{base}$  averaged over multiple DNS runs. Perturbations were time-stepped using linearised quasilinear (blue), linearised Navier-Stokes (orange) or full non-linear Navier-Stokes (green) equations. For each case, base flow was time-dependant and generated using full Navier-Stokes direct numerical simulations. Results shown for the symmetric S (top) and body-force driven BF2 (bottom) states. Black dashed lines are provided as guides to emphasise the zero gradient of the saturated states and to indicate the growth rate  $re(\sigma)$  of the unstable states. For comparison, the real part of the leading mEOS eigenvalue  $re(\sigma_{mEOS})$  is given for each of the states.

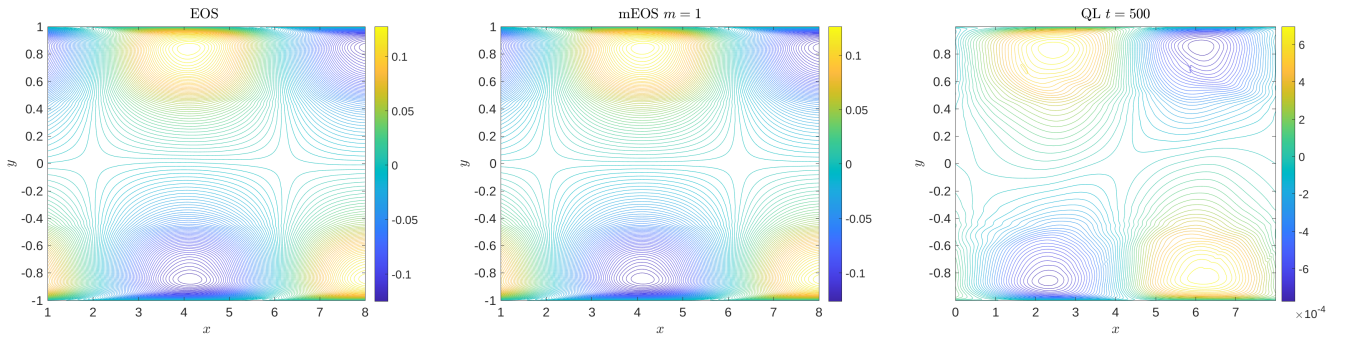


FIG. 11: Comparison of the leading eigenvectors from the EOS (left), mEOS  $m = 1$  (middle) analyses and an instantaneous snapshot of the velocity perturbation field in the QL experiment at  $t = 100$  (right) for the symmetric (S) state. Only the streamwise velocity component is shown. There is a good correspondence in the leading eigenvector across EOS and mEOS analyses and the QL experiment using a time-dependent base flow.



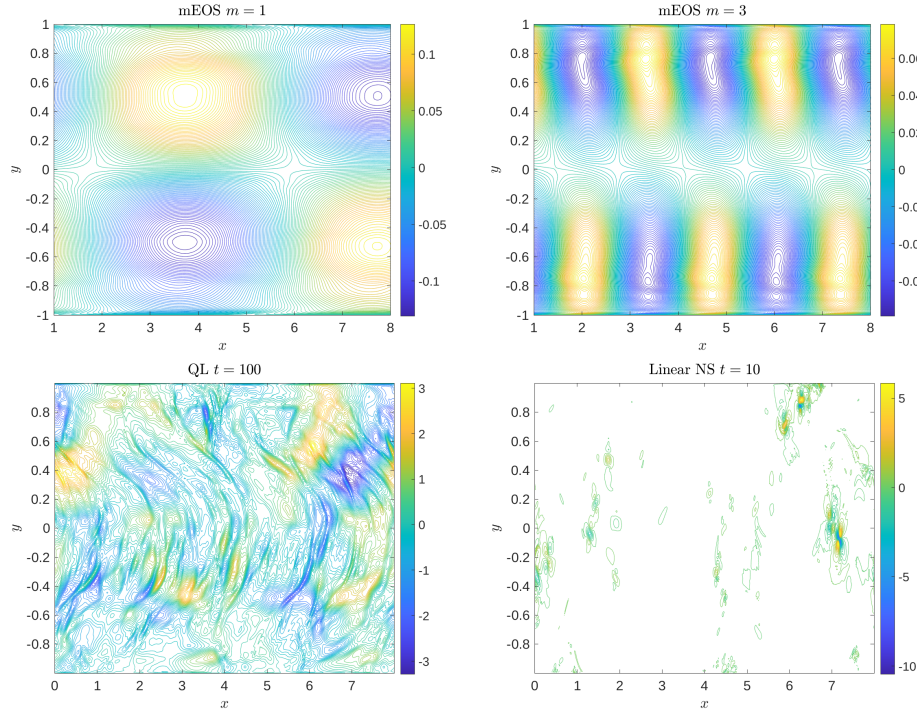


FIG. 12: Comparison of the leading eigenvectors from the mEOS  $m = 1$  (top left) and mEOS  $m = 3$  (top right) analysis with the instantaneous snapshots of the perturbation fields obtained from the QL experiment (bottom left) and linear NS experiment (bottom right) for the F2 state. The structures of the leading mEOS eigenvectors seem unrelated to the growing perturbations in the QL or LNS regimes.

time units (not shown). This behaviour is in contrast to what was found for state S where the perturbation saturated (see Figure 10 (top)). On the face of it, this experiment seems to show that state F2 is linearly unstable but this does not necessarily follow. Time-stepping a perturbation using the linearised Navier-Stokes equations (or in the tangent space of a turbulent attractor) can continually sample the stretching or contracting dynamics *along* the attractor which can dominate the anticipated decaying behaviour perpendicular to the attractor. It seems stretching along the attractor dominates for state F2 but not for state S. A comparison of the leading growing structures in Figure 12 is consistent with this: the QL and LNS flows bear no similarity with the predictions of mEOS. These LNS calculations for the state F2 highlight perfectly the difficulty in assessing the (linear) statistical stability using the Navier-Stokes equations touched on in the introduction.

Repeating the experiment (with  $E_{pert} = 10^{-5}E_{base}$ ) but now time-stepping the perturbation field with the full Navier-Stokes equations, we see the perturbation energy saturate after an initial transient: see Fig. 10 (bottom). Importantly, and as anticipated, the statistics of the turbulent state F2 recover albeit slowly. Figure 13 shows the relative difference between the correlation matrices averaged over a rolling time window between the perturbed and unperturbed F2 state. The statistical differences ebb away after an initial transient of growth. Since F2 is statistically linearly stable, this initial growth indicates that the statistical evolutionary operator linearised around the state F2 fixed point has to be non-normal. Finally, Fig. 14 shows the evolution of the streamwise perturbation velocity field. We see that the highly-localised structure visible at  $t = 10$  spreads in the channel at  $t = 20$  and reaches its saturated state at  $t = 30$  which does not change qualitatively even at much longer times  $t = 200$ . It takes much longer for the statistics to recover suggesting the adjustment along the attractor happens much quicker than normal to it: see Figure 13.

## VI. DISCUSSION

### A. Summary

We first summarise what has been done in the paper. The motivating objective has been to develop a theoretical approach which can assess the statistical stability of a turbulent state and goes beyond just examining the mean flow as Malkus did in the 1950s [1]. That such an approach should exist in some form is predicated on the fact that the statistics of a disturbed turbulent flow always return to their undisturbed values if the disturbance is not too large regardless of whether it decays or not. That is,

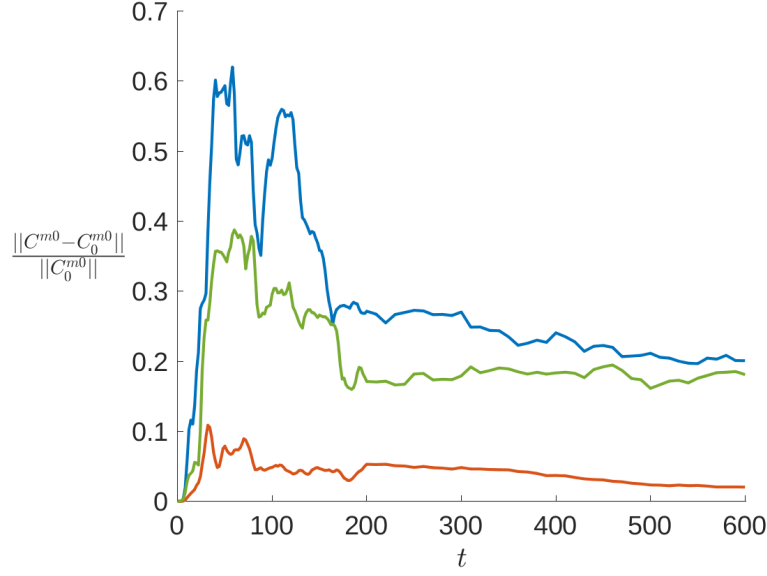


FIG. 13: Time evolution of the relative difference between correlation matrices of the full flow  $C^{m0}$  and base flow  $C_0^{m0}$  shown for  $m = 1$  (blue),  $m = 2$  (red) and  $m = 3$  (green). The correlation matrices were time-averaged over a rolling time window to display the statistical behaviour. Shown for the full non-linear NS experiment where the difference slowly approaches 0 signifying the recovery of the same statistical state.

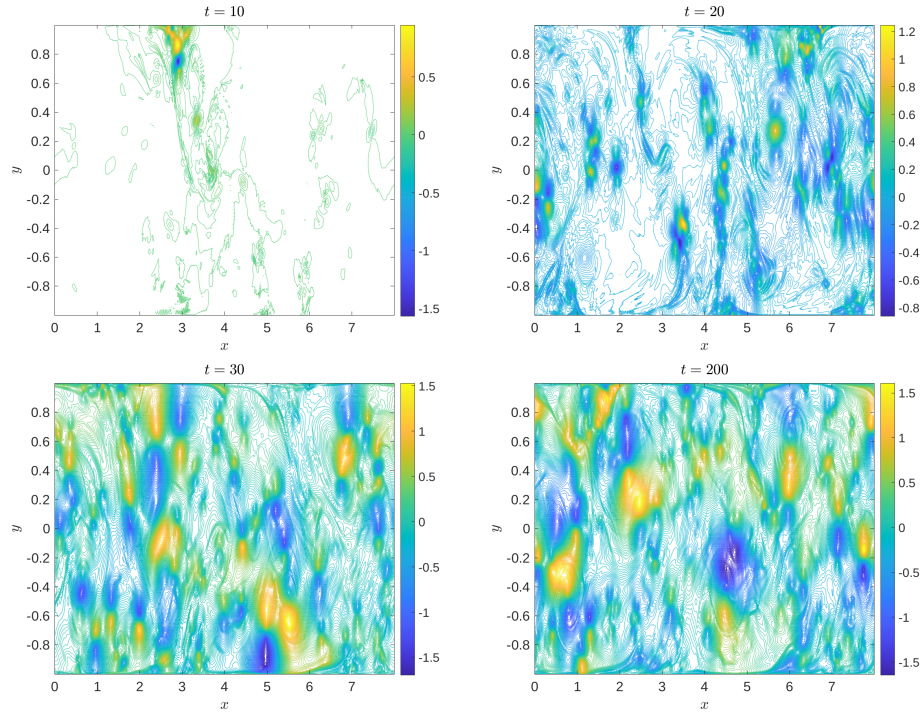


FIG. 14: Snapshots of the streamwise velocity component of the perturbation field taken from the full non-linear Navier-Stokes experiment with the F2 state. At time  $t = 10$  the unstable structure is still growing until time  $t = 20$  when it reaches its maximum size and starts to spread out through the channel, at time  $t = 30$  the perturbation saturates and shows no qualitative change at a much later time  $t = 200$ .

a turbulent flow is assumed *linearly* statistically stable (note this doesn't preclude the possibility of the statistical disturbance initially increasing before ultimately decaying away as the linear statistical operator may be non-normal). The way forward is to include more statistical information than just the mean of the flow in the analysis and the simplest such is the 2nd rank cumulant or 2-point equal-time correlations of the flow fluctuations. To do this, we have proposed to examine the statistical stability of the turbulent flow from within a cumulant equation framework truncated to just consider these statistical quantities (called CE2). Even in CE2, however, the ensuing statistical spectral problem is so unwieldy that a substitute has had to be sought. Here the well-known connection between CE2 and the Quasilinear (QL) equations can be exploited and we have argued that a suitably-designed QL spectral problem defined in §III can act as a good proxy to detect statistical instability. The key in designing this QL problem is to translate a statistically-steady base flow in CE2 into a representative *steady* base flow in the QL problem with no pretence that this base flow satisfies the QL equations itself.

The issue of how the statistical spectral problem in CE2 is related to the QL spectral problem is an intriguing one which seems not to have been discussed before. It is important because it underpins the tacit assumption that a CE2 simulation starting from given initial conditions should exactly shadow (statistically) the equivalent QL simulation given one is derivable from the other [e.g. 41, 43, 45]. However, this ignores the difference in dimensionality between the two formulations and the possibility of triggering unstable 'non-physical' perturbations in the larger CE2 problem (meaning perturbations which cannot exist in the QL setting). In §II E we have tried to clarify the different types of instability which exist in these formulations - Type A and B - and how they are related. In particular, for Type A instabilities, the spectral QL problem captures the most unstable disturbance possible in the CE2 system and so is an accurate proxy for CE2: CE2 can only be Type A unstable if QL is. For Type B, the situation is less certain. While it remains the case that any Type B instability in QL is mirrored in CE2 and CE2 will likely have further Type B instabilities, it is not clear whether CE2 can have a Type B instability and QL not. Given the as-yet-unreported consequence of this - CE2 could suffer a bifurcation away from QL - it is tempting to assume that this is not possible and then that QL also is a good proxy for Type B perturbations. With this one caveat, probing the QL spectral problem - named here Extended Orr-Sommerfeld analysis (EOS) - then appears the best way to examine the statistical stability of a flow where the 2-pt correlations as well as the mean profile of the flow are incorporated.

Despite improving upon the CE2 spectral problem, EOS is still unfortunately quite costly to implement so a reduced version was proposed in §III A - minimally Extended Orr-Sommerfeld analysis (mEOS) - which has a similar cost to the usual Orr-Sommerfeld analysis of the flow mean. mEOS was found to capture the qualitative effect of EOS with either both producing an improved estimate of statistical stability (e.g. the  $m = 2$  mode for state F1: see figure 5 bottom left) or offering no correction of the OS eigenvalue (e.g. the  $m = 1$  mode for state F1). Reassuringly, both approaches never made a poorer statistical stability prediction than OS analysis at least over the turbulent channel flow states tested.

## B. Implications

By incorporating 2-pt fluctuation correlations, EOS and its slimmed down version mEOS represent an attempt to generate a better way to assess the statistical stability of a turbulent flow than just considering the mean profile. Malkus (1956) wanted to use this to constrain the set of realisable turbulent mean profiles and it still remains an interesting requirement given the paucity of predictive alternatives. The concept of marginal stability still periodically rears its head in the literature to post-rationalise turbulent mean profiles (e.g see [69] and references therein) and EOS represents a finer tool for this. As noted in the introduction, the mean flow is increasingly taken as the starting point for resolvent flow analysis. To move this towards a full wall-bounded turbulence theory, a way has to be found to close the cycle between the fluctuation field and the mean. Just maybe, requiring statistical stability with respect to the dominant fluctuation fields could help constrain this.

A byproduct of this work is that it has also suggested an improved approach for predicting coherent structures in turbulent flows. Initial work [13–15] linearising around the turbulent mean proved successful in free shear flows but less so when viscosity plays a leading role. Admittedly, EOS or mEOS needs extra (second cumulant) information about the base flow which adds cost to the analysis but the potential for better predictions is clear. A popular (cheap) alternative approach has been to apply OS analysis around the mean profile which incorporates an eddy viscosity to acknowledge the presence of the base fluctuations [6–8, 25, 26, 29, 30]. This eddy viscosity is taken to be that which is needed to sustain the turbulent mean profile and so makes no attempt to incorporate fluctuation information for each excited wavenumber of the base flow as in EOS. In the well-known triple expansion of Hussain & Reynolds [70], the coherent wave part ( $\tilde{f}$  in their equation (1.1)) is the equivalent of the steady modelling flow  $[\tilde{\mathbf{u}}_0]^{mm}$  for each wavenumber pairing present. The difference is their base flow part is driven and so time-periodic whereas ours is undriven but made steady to permit a standard eigenvalue approach to analyse stability. Retaining some time-periodicity in  $\tilde{\mathbf{u}}_0$  would necessitate a much more demanding Floquet analysis but is, in principle, possible.

The cumulant framework examined here to motivate EOS was used only to the first non-trivial level where only the first and second cumulants are retained. Whether this represents a good approximation or not to modelling the turbulent flow itself is a question not considered here. Rather the focus is on the associated spectral problem characterising the statistical stability *within* this framework *taking* the turbulent base flow as a given. Clearly considering higher cumulants beyond the the second would

be better but the computational cost of handling the ensuing spectral problem becomes prohibitive. Interestingly, ‘projecting down’ to an underlying Navier-Stokes-type problem fails immediately unless no closure at all is performed which means  $CE_\infty$  is considered. This gives what we have called the infinitely Extended Orr-Sommerfeld analysis (iEOS) which is as costly as EOS and unfortunately does not have a ‘minimal’ version. Again, only targeting certain subsets of fluctuation fields - e.g. key triads suggested by resolvent flow analysis - may yet make this tractable.

### C. Future perspectives

In terms of future work, an obvious focus is to improve the main approximation in EOS which is deriving a representative base flow. Here, we have used the leading singular vector of the second cumulant for each excited (vector) wavenumber but other strategies involving information from higher order cumulants are certainly possible (leaving aside the cost of computing these...). This would seem sensible in the case of iEOS which is a proxy for  $CE_\infty$  where *all* the cumulants are retained and the only other cumulant system beyond CE2 which allows a Navier-Stokes-type proxy. Pragmatically, a steady base flow has been sought which leads to a (conceptually) simple eigenvalue problem. Trying to go beyond this profoundly complicates matters.

One interesting future direction hinted at in the introduction is to relax the averaging procedure to just being over the stream-wise direction or, more generally, redefine what constitutes the ‘mean’. A key feature we have been able to exploit is the connection between CE2 and the QL equations which still holds if the mean is more flexibly defined to include some wavenumber subset of the fluctuation field. The then ‘generalised’ QL equations [58] have the advantage of including more of the nonlinearity in the Navier-Stokes equations and can interpolate between the QL equations and the full Navier Stokes equations depending on how the mean is defined. A minimal mean extension would be to include one spanwise wavenumber field (in the spirit of [70]) whereas including *all* fluctuation fields with no streamwise variation is equivalent to a mean defined by only streamwise averaging. There are many theoretical reasons for considering the latter, where the mean is  $U(y,z)\hat{\mathbf{x}}$  rather just  $U(y)\hat{\mathbf{x}}$ , in wall-bounded flows (e.g. the SSP/VWI mechanism [71, 72]) but capturing it experimentally is very time-consuming task and using it reduces the predictive power of resolvent flow analysis. Even in computations, the spanwise homogeneity needs to be broken otherwise there is no reason to suppose the mean flow should not be spanwise-invariant (and then the spanwise structure of the mean profile needs to be divorced from the source of spanwise inhomogeneity). Nevertheless, this choice is starting to receive attention at least at the level of doing OS analysis on  $U(y,z)\hat{\mathbf{x}}$  (see [51] and references herein) and this analysis can be extended as envisaged here.

Many challenges remain. Statistical stability is an important fundamental feature of turbulent flows yet is difficult to assess and hence to exploit. Hopefully, the work reported here represents a useful but admittedly small step forward.

Acknowledgements: VM gratefully thanks EPSRC for the PhD studentship which supported her during this work.

### Appendix: Solving the eigenvalue problem

Here we explain how we implemented mEOS and EOS calculations as an eigenvalue problem in 2D channel flow. We expand fluctuation field in terms of sine and cosine modes:

$$\tilde{\mathbf{u}}(x, y, t) := \sum_{m=1}^{N_x} \left( \tilde{\mathbf{u}}_c^{m0}(y, t) \cos(m\alpha x) + \tilde{\mathbf{u}}_s^{m0}(y, t) \sin(m\alpha x) \right) \quad (\text{A.1})$$

The non-linear term in the mean equation then becomes:

$$(\overline{\tilde{u}\tilde{v}})_y = \frac{1}{2} \partial_y \sum_{m=1}^{N_x} \left( \tilde{u}_c^{m0} \tilde{v}_c^{m0} + \tilde{u}_s^{m0} \tilde{v}_s^{m0} \right). \quad (\text{A.2})$$

The Extended Orr-Sommerfeld equations then take the following form:

$$\partial_t \delta U = \frac{1}{Re} \partial_y^2 \delta U + \delta G - \frac{1}{2} \partial_y \sum_{m=1}^{N_x} \left( \delta \tilde{u}_c^{m0} \tilde{v}_c^{m0} + \tilde{u}_c^{m0} \delta \tilde{v}_c^{m0} + \delta \tilde{u}_s^{m0} \tilde{v}_s^{m0} + \tilde{u}_s^{m0} \delta \tilde{v}_s^{m0} \right), \quad (\text{A.3})$$

and for each wavenumber  $(m, 0)$ :

$$\partial_t \delta \tilde{u}_c^{m0} = \frac{1}{Re} (\partial_y^2 - m^2) \delta \tilde{u}_c^{m0} - m \delta \tilde{p}_s^{m0} - m U \delta \tilde{u}_s^{m0} - U_y \delta \tilde{v}_c^{m0} - m \delta U \tilde{u}_{0s}^{m0} - \delta U_y \delta \tilde{v}_{0c}^{m0} \quad (\text{A.4})$$

$$\partial_t \delta \tilde{u}_s^{m0} = \frac{1}{Re} (\partial_y^2 - m^2) \delta \tilde{u}_s^{m0} + m \delta \tilde{p}_c^{m0} + m U \delta \tilde{u}_c^{m0} - U_y \delta \tilde{v}_s^{m0} + m \delta U \tilde{u}_{0c}^{m0} - \delta U_y \delta \tilde{v}_{0s}^{m0} \quad (\text{A.5})$$

$$\partial_t \delta \tilde{v}_c^{m0} = \frac{1}{Re} (\partial_y^2 - m^2) \delta \tilde{v}_c^{m0} - \partial_y \delta \tilde{p}_c^{m0} - m U \delta \tilde{v}_s^{m0} - m \delta U \tilde{v}_{0s}^{m0} \quad (\text{A.6})$$

$$\partial_t \delta \tilde{v}_s^{m0} = \frac{1}{Re} (\partial_y^2 - m^2) \delta \tilde{v}_s^{m0} - \partial_y \delta \tilde{p}_s^{m0} + m U \delta \tilde{v}_c^{m0} + m \delta U \tilde{v}_{0c}^{m0} \quad (\text{A.7})$$

$$m \tilde{u}_s^{m0} + \partial_y \tilde{v}_c^{m0} = 0 \quad (\text{A.8})$$

$$-m \tilde{u}_c^{m0} + \partial_y \tilde{v}_s^{m0} = 0 \quad (\text{A.9})$$

This eigenvalue problem is real and so eigenvalues are either real or come in complex conjugate pairs where a real physical velocity field is formed by addition:

$$\begin{bmatrix} \delta U \\ \vdots \\ \delta \tilde{u}_c^{m0} \cos(m\alpha x) \\ \delta \tilde{u}_s^{m0} \sin(m\alpha x) \\ \vdots \end{bmatrix} e^{\lambda t} + \begin{bmatrix} \delta U^* \\ \vdots \\ \delta \tilde{u}_c^{*m0} \cos(m\alpha x) \\ \delta \tilde{u}_s^{*m0} \sin(m\alpha x) \\ \vdots \end{bmatrix} e^{\lambda^* t}. \quad (\text{A.10})$$

- 
- [1] W. V. R. Malkus, Outline of a theory of turbulent shear flow, *Journal of Fluid Mechanics* **1**, 521 (1956).
  - [2] W. M. Orr, The stability or instability of the steady motions of a perfect liquid and of a viscous liquid. part ii: A viscous liquid, *Proceedings of the Royal Irish Academy. Section A: Mathematical and Physical Sciences* **27**, 69 (1907).
  - [3] A. Sommerfeld, Ein beitrag zur hydrodynamische erklärung der turbulenten flussigkeitsbewegungen, *Proceedings of the 4th International Congress of Mathematicians (Rome)* **V. III.**, 116–124 (1908).
  - [4] W. C. Reynolds and W. G. Tiederman, Stability of turbulent channel flow, with application to Malkus's theory, *Journal of Fluid Mechanics* **27**, 253 (1967).
  - [5] A. S. Iyer, F. D. Witherden, S. I. Chernyshenko, and P. E. Vincent, Identifying eigenmodes of averaged small-amplitude perturbations to turbulent channel flow, *Journal of Fluid Mechanics* **875**, 758 (2019).
  - [6] W. C. Reynolds and A. K. M. F. Hussain, The mechanics of an organised wave in turbulent shear flow. part 3. theoretical models and comparisons with experiments, *J. Fluid Mech.* **54**, 263 (1972).
  - [7] P. K. Sen and S. V. Veeravalli, Behaviour of organised disturbances in fully developed turbulent channel flow, *Sadhana* **25**, 423 (2000).
  - [8] P. K. Sen, S. V. Veeravalli, P. W. Carpenter, and G. Joshi, Organised structures in wall turbulence as deduced from stability theory-based methods, *Sadhana* **32**, 51 (2007).
  - [9] W. V. R. Malkus, Turbulent velocity profiles from stability criteria, *Journal of Fluid Mechanics* **90**, 401 (1979).
  - [10] W. V. R. Malkus, Statistical stability criteria for turbulent flow, *Physics of Fluids* **8**, 1582 (1996).
  - [11] W. V. R. Malkus, Borders of disorder: in turbulent channel flow, *Journal of Fluid Mechanics* **489**, 185 (2003).
  - [12] N. Nikitin, Characteristics of the leading Lyapunov vector in turbulent channel flow, *Journal of Fluid Mechanics* **849**, 942 (2018).
  - [13] D. G. Crighton and M. Gaster, Stability of slowly diverging jet flow, *Journal of Fluid Mechanics* **77**, 397 (1976).
  - [14] M. Gaster, E. Kit, and I. Wygnanski, Large-scale structures in a forced turbulent mixing layer, *Journal of Fluid Mechanics* **150**, 23 (1985).
  - [15] A. Roshko, Instability and turbulence in shear flows, *Theoretical and Applied Mechanics 1992*, 1 (1993).
  - [16] L. Lesshafft, P. Huerre, P. Sagaut, and M. Terracol, Nonlinear global modes in hot jets, *J. Fluid Mech.* **554**, 393 (2006).
  - [17] D. Barkley, Linear analysis of the cylinder wake mean flow, *Europhys. Lett.* **75**, 750 (2006).
  - [18] D. Sipp and A. Lebedev, Global stability of base and mean flows: a general approach and its applications to cylinder and open cavity flows, *Journal of Fluid Mechanics* **593**, 333–358 (2007).
  - [19] E. Akervik, U. Ehrenstein, F. Gallaire, and D. S. Henningson, Global two-dimensional stability measures of the flat plate boundary-layer flow, *Eur. J. Mechanics B* **27**, 501 (2008).
  - [20] D. Sipp, O. Marquet, P. Meliga, and A. Barbagallo, Dynamics and control of global instabilities in open-flows: a linearized approach, *Applied Mechanics Reviews* **63**, 030801 (2010).
  - [21] V. Mantic-Lugo, C. Arratia, and F. Gallaire, Self-consistent mean flow description of the nonlinear saturation of the vortex shedding in a cylinder wake, *Phys. Rev. Lett.* **113**, 084501 (2014).
  - [22] S. Beneddine, D. Sipp, A. Arnault, J. Dandois, and L. Lesshafft, Conditions for validity of mean flow stability analysis, *Journal of Fluid Mechanics* **798**, 485–504 (2016).
  - [23] A. Lefauve, J. L. Partridge, Q. Zhou, S. B. Dalziel, C. P. Caulfield, and P. F. Linden, The structure and origin of confined Holmboe waves, *Journal of Fluid Mechanics* **848**, 508 (2018).
  - [24] K. M. Butler and B. F. Farrell, Optimal perturbations and streak spacing in wall-bounded turbulent shear flow, *Phys. Fluids* **5**, 774 (1993).

- [25] J. C. del Alamo and J. Jimenez, Linear energy amplification in turbulent channels, *J. Fluid Mech.* **559**, 205 (2006).
- [26] C. Cossu, G. Pujals, and S. Depardon, Optimal transient growth and very large structures in turbulent boundary layers, *J. Fluid Mech.* **619**, 79 (2009).
- [27] M. R. Jovanovic and B. Bamieh, Componentwise energy amplification in channel flows, *J. Fluid Mech.* **534**, 143 (2005).
- [28] S. I. Chernyshenko and M. F. Baig, The mechanism of streak formation in near-wall turbulence, *Journal of Fluid Mechanics* **544**, 99 (2005).
- [29] Y. Hwang and C. Cossu, Amplification of coherent streaks in the turbulent couette flow: an input–output analysis at low reynolds number, *J. Fluid Mech.* **643**, 333 (2010).
- [30] Y. Hwang and C. Cossu, Linear non-normal energy amplification of harmonic and stochastic forcing in the turbulent channel flow, *J. Fluid Mech.* **664**, 51 (2010).
- [31] B. J. McKeon and A. S. Sharma, A critical-layer framework for turbulent pipe flow, *J. Fluid Mech.* **658**, 336 (2010).
- [32] R. Moarref and M. R. Jovanovic, Model-based design of transverse wall oscillations for turbulent drag reduction, *Journal of Fluid Mechanics* **707**, 205 (2012).
- [33] O. Blesbois, S. I. Chernyshenko, S. I. Toubert, and M. A. Leschziner, Pattern prediction by linear analysis of turbulent flow with drag reduction by wall oscillation, *Journal of Fluid Mechanics* **724**, 607 (2013).
- [34] A. S. Sharma and B. J. McKeon, On coherent structure in wall turbulence, *J. Fluid Mech.* **728**, 196 (2013).
- [35] O. T. Schmidt, A. Towne, G. Rigas, T. Colonius, and G. A. Bres, Spectral analysis of jey turbulence, *J. Fluid Mech.* **855**, 953 (2018).
- [36] B. McKeon, The engine behind (wall) turbulence: perspectives on scale interactions, *Journal of Fluid Mechanics* **817**, P1 (2017).
- [37] E. Hopf, Statistical hydromechanics and functional calculus, *Journal of Rational Mechanics and Analysis* **1**, 87 (1952).
- [38] S. A. Orszag, Statistical theory of turbulence, in *Fluid Dynamics, Les Houches 1973*, eds. R. Balian & J. L. Peube, Gordon & Breach, New York (1977).
- [39] U. Frisch, *Turbulence*, Cambridge University Press (1995).
- [40] B. F. Farrell and P. J. Ioannou, Structural stability of turbulent jets, *Journal of Atmospheric Sciences* **60**, 2101 (2003).
- [41] J. B. Marston, E. Conover, and T. Schneider, Statistics of an unstable barotropic jet from a cumulant expansion, *Journal of Atmospheric Sciences* **65**, 1955 (2008).
- [42] K. Srinivasan and W. R. Young, Zonostrophic Instability, *Journal of Atmospheric Sciences* **69**, 1963 (2012).
- [43] S. M. Tobias and J. B. Marston, Direct statistical simulation of out-of-equilibrium jets, *Phys. Rev. Lett.* **110**, 104502 (2013).
- [44] J. B. Parker and J. A. Krommes, Generation of zonal flows through symmetry breaking of statistical homogeneity, *New Journal of Physics* **16**, 035006 (2014).
- [45] S. M. Tobias, K. Dagon, and J. B. Marston, Astrophysical fluid dynamics via direct statistical simulation, *Ap. J.* **727**, 127 (2011).
- [46] B. F. Farrell and P. J. Ioannou, A stochastic structural stability theory model of the drift wave-zonal flow system, *Phys. of Plasmas* **16**, 112903 (2009).
- [47] J. B. Parker and J. A. Krommes, Zonal flow as pattern formation, *Phys. Plasmas* **20**, 100703 (2013).
- [48] B. F. Farrell and P. J. Ioannou, Dynamics of streamwise rolls and streaks in turbulent wall-bounded shear flow, *Journal of Fluid Mechanics* **708**, 149–196 (2012).
- [49] N. C. Constantinou, A. Lozano-Duran, M.-A. Nikolaidis, B. F. Farrell, P. J. Ioannou, and J. Jimenez, Turbulence in the highly restricted dynamics of a closure at second order: comparison with DNS, *Journal of Physics Conference Series* **506**, 012004 (2014).
- [50] B. F. Farrell, P. J. Ioannou, J. Jimenez, N. C. Constantinou, A. Lozano-Duran, and M.-A. Nikolaidis, A statistical state dynamics-based study of the structure and mechanism of large-scale motions in plane Poiseuille flow, *Journal of Fluid Mechanics* **809**, 290 (2016).
- [51] A. Lozano-Duran, N. C. Constantinou, M.-A. Nikolaidis, and M. Karp, Cause-and-effect of linear mechanisms sustaining wall turbulence, *J. Fluid Mech.* **914**, A8 (2021).
- [52] V. E. P. Vedenov, A. A. and R. Z. Sagdeev, Quasilinear theory of plasma oscillations, *Proceedings of IAEA conference on Plasma Physics and Controlled Nuclear Fusion Research*, 465 (1961).
- [53] J. R. Herring, Investigation of problems in thermal convection, *J. Atmos. Sci.* **20**, 325 (1963).
- [54] J. R. Herring, Investigation of problems in thermal convection - rigid boundaries, *J. Atmos. Sci.* **21**, 277 (1964).
- [55] C. G. Hernandez and Y. Hwang, Spectral energetics of a quasilinear approximation in uniform shear turbulence, *J. Fluid Mech.* **904**, A11 (2020).
- [56] M. J. B. Skitka, J. and B. Fox-Kemper, Reduced-order quasilinear model of ocean boundary-layer turbulence, *Journal of Physical Oceanography* **50**, 537 (2020).
- [57] L. O'Connor, D. Lecoanet, and E. H. Anders, Marginally stable thermal equilibria of Rayleigh-Benard convection, *Physical Review Fluids* **6**, 093501 (2021).
- [58] J. B. Marston, G. P. Chini, and S. M. Tobias, Generalized Quasilinear Approximation: Application to Zonal Jets, *Physical Review Letters* **116**, 10.1103/PhysRevLett.116.214501 (2016).
- [59] C. G. Hernandez, Q. Yang, and Y. Hwang, Generalised quasilinear approximations of turbulent channel flow: Part 1. streamwise nonlinear energy transfer, *arXiv:2108.12395* (2021).
- [60] V. K. Markeviciute and R. R. Kerswell, Degeneracy of turbulent states in two-dimensional channel flow, *Journal of Fluid Mechanics* **917**, A57 (2021).
- [61] H. B. Squire, On the stability for three-dimensional disturbances of viscous fluid flow between parallel walls, *Proc. Roy. Soc. Lond.* **142**, 621 (1933).
- [62] R. R. Kerswell, Recent progress in understanding the transition to turbulence in a pipe, **18**, R17 (2005).
- [63] B. Eckhardt, T. M. Schneider, and J. Westerweel, Turbulence transition in pipe flow, *Ann. Rev. Fluid Mech.* **39**, 447 (2007).
- [64] G. Kawahara, M. Uhlmann, and L. van Veen, The significance of simple invariant solutions in turbulent flows, *Ann. Rev. Fluid Mech.* **44**, 203 (2012).

- [65] M. D. Graham and D. Floryan, Exact coherent states and the nonlinear dynamics of wall-bounded turbulent flows , *Ann. Rev. Fluid Mech.* **53**, 227 (2021).
- [66] J. B. Marston, W. Qi, and S. M. Tobias, Direct statistical simulation of a jet, in ‘Jonal Jets’ Cambridge University Press , 332 (2019).
- [67] K. J. Burns, G. M. Vasil, J. S. Oishi, D. Lecoanet, and B. P. Brown, Dedalus: A flexible framework for numerical simulations with spectral methods, *Physical Review Research* **2**, 023068 (2020), arXiv:1905.10388 [astro-ph.IM].
- [68] G. Falkovich and N. Vladimirova, Turbulence appearance and nonappearance in thin fluid layers, *Phys. Rev. Lett.* **121**, 164501 (2018).
- [69] H. J. Brauckmann and B. Eckhardt, Marginally stable and turbulent boundary layers in low-curvature Taylor-Couette flow, *Journal of Fluid Mechanics* **815**, 149 (2017).
- [70] A. K. M. F. Hussain and W. C. Reynolds, The mechanics of an organised wave in turbulent shear flow, *Journal of Fluid Mechanics* **41**, 241 (1970).
- [71] F. Waleffe, On a self-sustaining process in shear flows, *Physics of Fluids* **9**, 883 (1997).
- [72] P. Hall and S. Sherwin, Streamwise vortices in shear flows: harbingers of transition and the skeleton of coherent structures, *Journal of Fluid Mechanics* **661**, 178 (2010).